Computational Analysis of Dynamical Responses to the Intrinsic Pathway of Programmed Cell Death

Tongli Zhang, Paul Brazhnik, and John J. Tyson*
Department of Biological Science, Virginia Polytechnic Institute and State University, Blacksburg Virginia

ABSTRACT Multicellular organisms shape development and remove aberrant cells by programmed cell death ("apoptosis"). Because defective cell death (too little or too much) is implicated in various diseases (like cancer and autoimmunity), understanding how apoptosis is regulated is an important goal of molecular cell biologists. To this end, we propose a mathematical model of the intrinsic apoptotic pathway that captures three key dynamical features: a signal threshold to elicit cell death, irreversible commitment to the response, and a time delay that is inversely proportional to signal strength. Subdividing the intrinsic pathway into three modules (initiator, amplifier, executioner), we use computer simulation and bifurcation theory to attribute signal threshold and time delay to positive feedback in the initiator module and irreversible commitment to positive feedback in the executioner module. The model accounts for the behavior of mutants deficient in various genes and is used to design experiments that would test its basic assumptions. Finally, we apply the model to study p53-induced cellular responses to DNA damage. Cells first undergo cell cycle arrest and DNA repair, and then apoptosis if the damage is beyond repair. The model ascribes this cell-fate transition to a transformation of p53 from "helper" to "killer" forms.

INTRODUCTION

Homeostasis of multicellular organisms is maintained by a delicate balance between cell proliferation and death. Programmed cell death (apoptosis) is used by organisms to remove unwanted cells during embryonic development and immune system maturation, and to remove aberrant cells that are damaged, infected, or transformed. Failure to trigger apoptosis can lead to accumulation of damaged DNA and increased risk of tumor progression (1,2). On the other hand, over-active apoptosis causes unnecessary cell loss, resulting in cardiovascular and neurodegenerative diseases. Thus, understanding the regulation of apoptosis is an important goal of basic research in biology and medicine, especially in the field of molecular oncology (3).

Apoptosis is initiated and executed by a family of proteases called caspases, meaning "cysteine proteases with specificity for aspartic acid residue". Caspases are present in normal cells in inactive forms called procaspases. In response to appropriate signals, procaspases are cleaved to active forms and proceed to disassemble the cell from inside. In addition to degrading cellular proteins, caspases activate DNases that destroy the cell's genome.

Cells employ two interrelated pathways to trigger programmed cell death (Fig. 1). (The nomenclature we use for protein components of apoptotic pathways is explained in Tables 1 and 2.) The intrinsic pathway responds to intracellular stresses (hypoxia, DNA damage, etc.) by activating BH3 proteins, a class of proapoptotic proteins possessing only one BCL2-homology structural domain. Once elevated, BH3 proteins promote the activation of other proapoptotic proteins, BAX and BAK, by sequestering inhibitors of BAX and BAK, and in some cases (the BH3 proteins BID and BIM) by causing a conformational change of BAX. Activated BAX and BAK form oligomers in the mitochondrial outer membrane, increasing its permeability to cytochrome *c* and the second mitochondria-driven activator of caspase (SMAC). In the cytoplasm, cytochrome *c* binds to APAF-1 to form an apoptosome, which activates caspase 9. Caspase 9 then activates the executioner, caspase 3 (4). SMAC promotes apoptosis by inhibiting XIAP, an inhibitor of caspase 3 and caspase 9.

The extrinsic pathway responds to extracellular death ligands (e.g., TNFα) by activating caspases 8 and 10, which in turn activate executioner caspases 3, 6, and 7 (5,6). In addition to activating caspase 3 directly, caspase 8 also stimulates the intrinsic pathway by activating BID (4). In this manuscript, we concentrate on the intrinsic pathway.

Apoptosis has three characteristic physiological features:

1. The cell death response must not be triggered by weak signals. Procaspases are present in all normal cells. To survive in a noisy environment, cells must keep these caspases inactive in the face of minor fluctuations in the intrinsic and extrinsic pathways. Apoptosis should be triggered only when the stress level is above some specific threshold.
2. Once apoptosis is triggered, cells should commit to finishing the process. Caspases destroy the genome and disrupt cellular structure. To abandon the process half way could be very dangerous to the organism, generating damaged cells that might develop into tumors.
3. There is a characteristic time delay between signal and response: the larger the stress, the shorter the time delay before apoptosis (7,8).

Programmed cell death is controlled by a complex network of interacting genes and proteins. Feed forward and feedback

Submitted September 29, 2008, and accepted for publication April 29, 2009.

*Correspondence: tyson@vt.edu

Editor: Arup Chakraborty.

0006-3495/09/07/0415/20 $2.00

doi: 10.1016/j.bpj.2009.04.053

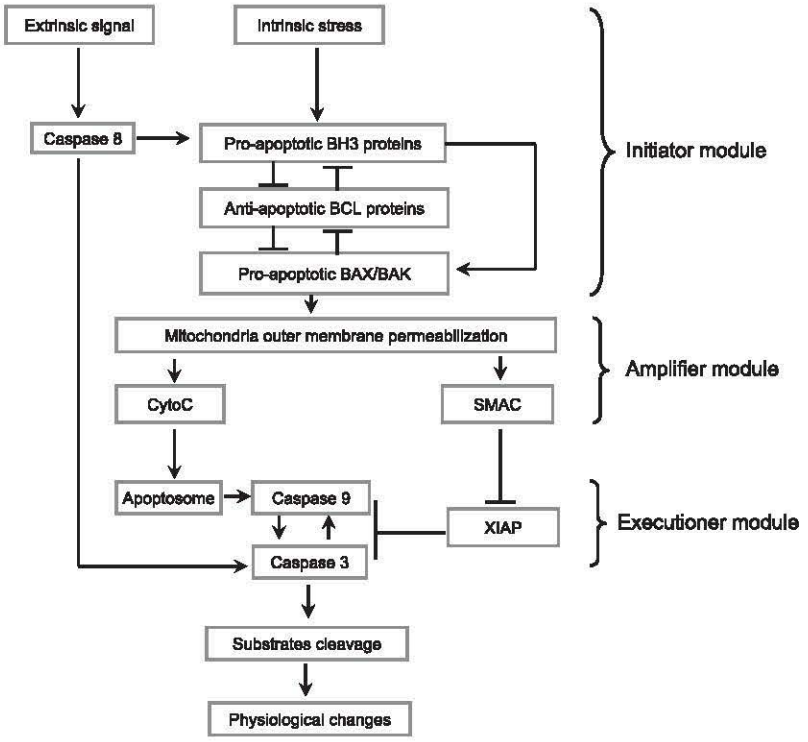

FIGURE 1 Flow chart of the apoptotic program. Arrows and bars indicate activation and inhibition, respectively. See text for details.

signals in the network make the dynamic features of the control system difficult to comprehend intuitively and to predict reliably by verbal argument alone. To deal with such complexity, several investigators have constructed quantitative (mathematical) models to investigate the regulation of programmed cell death in a rigorous and systemic manner (7,9–19). Building on prior work, we present a model of the intrinsic pathway that addresses specifically the dynamical basis of the three characteristic physiological features of apoptosis. We subdivide the intrinsic pathway into three modules (initiator, amplifier, and executioner modules) and show how positive feedback in the initiator module is responsible for the signal threshold and the time delay, and how the executioner module ensures commitment to cell death. Numerical simulations of the model are supplemented by bifurcation analyses that reveal the essential dynamical features of the network. We also consider how regulation can go awry under specific circumstances.

Using this model of apoptotic regulation, we seek to understand how cells decide between life and death after DNA damage. Cells respond to DNA damage by activating a transcription factor, p53. At first, p53 promotes cell survival by inducing transcription of genes for cell cycle arrest and for DNA damage repair, thereby giving cells a chance to repair the damage before it is propagated to a new generation of cells. If the damage is beyond repair, p53 induces apoptosis in multiple ways. How p53 chooses between life and death has been puzzling for a long time (20–22). In this manuscript, we propose a possible mechanism for the life-or-death decision. Transient damage promotes p53 in a "helper" form, which induces cell cycle arrest and damage repair. Sustained DNA damage transforms p53 to a "killer" form that induces apoptosis. Analysis and simulation of the model show how p53 helpers and killers might interact with each other in the cell-fate decision. The model also makes testable predictions as to how the decision can be perturbed.

Model assumptions and molecular justifications

We subdivide the intrinsic pathway into three modules (Fig. 2): the initiator module takes a stress signal as input and outputs mitochondrial BAX level, the amplifier module describes how mitochondrial BAX causes the release of cytochrome *c* (CytoC) and SMAC, and the executioner module describes how CytoC and SMAC cooperate to activate caspase 3.

In building the model we must continually make decisions about what level of detail to keep and what to ignore. We desire a model that is general enough to apply to real death decisions made by cells but simple enough to yield to tools of mathematical analysis (bifurcation theory) and flexible enough to be tailored (in future) to specific cell types and experimental circumstances. For example, in the model presented here, we consider BH3 proteins as a general class of proapoptotic agents that work by activating BAX proteins, and we assume (Fig. 2 *A*) that a stress signal drives the production of active BH3 proteins. Later, when appropriate, we can incorporate details of how specific BH3 proteins are activated by different stresses. For example, NOXA, PUMA, and BIM levels are upregulated by p53-dependent transcriptional activation in response to DNA damage (23), whereas BID is activated by caspase-8-dependent cleavage in response

TABLE 1 Model components

Notation	Explanation
aC9	Active caspase 9, p35/p10
ARF	Alternative reading frame of CDKN2A (cyclin-dependent kinase inhibitor 2A)
ARF/MDM2	Dimer of ARF and MDM2
ASPP	Apoptosis-stimulating protein of p53
BAX	BCL2-associated X protein
BAXm	Active BAX, inserted in mitochondrial outer membrane
BAXm/BCL2	Dimer of BAXm and BCL2
BCL2	Class of antiapoptotic BCL subfamily proteins
BH3	Class of proapoptotic BH3-only subfamily proteins
BH3/BCL2	Dimer of BH3 and BCL2
BH3AC	BH3 activators: BIM and t-BID
BH3AC/BCL2	Dimer of BH3AC and BCL2
BH3DR	BH3 de-repressors: PUMA, NOXA, BMF, etc.
BH3DR/BCL2	Dimer of BH3DR and BCL2
C3	Active form of caspase 3
C9	Caspase 9, p35/p12
CC, CO	Closed and open states of mitochondrial channels
CycE	Cyclin E
CytoC	Cytochrome *c* in cytoplasm
CytoCmito	Cytochrome *c* in mitochondria
E2F1	Transcription factor
MDM2	Mouse double minute 2 homolog
p21	Cyclin-dependent kinase inhibitor
p21/CycE	Dimer of p21 and cyclin E
p53	Transcription factor, tumor suppressor protein
p73	Member of p53 family
RB	Retinoblastoma protein
RB/E2F1	Dimer of RB and E2F1
RBP	Phosphorylated RB protein
SMAC	Second mitochondria-driven activator of caspase, in cytoplasm
SMAC/XIAP	Dimer of SMAC and XIAP
SMACmito	SMAC in mitochondria
XIAP	X-linked inhibitor of apoptosis protein

TABLE 2 Other proteins of interest

Protein name	Description
AIF	Apoptosis-inducing factor
BID	BH3-interacting domain death agonist
BIM	Bcl-2 interacting mediator of cell death.
BMF	Bcl2-modifying factor
BRN3A, B	POU-domain transcription factors
CD95 and Fas	Tumor necrosis factor receptor superfamily, member 6
c-FLIP	Caspase 8- and FADD-like apoptosis regulator
DR5	Tumor necrosis factor receptor superfamily, member 10b
DYRK2	Dual-specificity tyrosine-phosphorylation-regulated kinase 2
HZF	Hematopoietic zinc finger
IGF-BP3	Insulinlike growth-factor-binding protein
JMY	Junction-mediating and regulatory protein
NOXA	PMAIP1 (phorbol-12-myristate-13-acetate-induced protein 1)
P53AIP1	p53-regulated apoptosis-inducing protein 1
P53DINP1	p53-dependent damage-inducible nuclear protein 1
PIG3	p53-induced gene 3
PTEN	Phosphatase and tensin homolog
PUMA	p53 upregulated modulator of apoptosis

to an external death signal like TNFα (4). We hope that readers will approve the spirit in which these modeling decisions have been made, and will see how to tailor the model to new situations by adding appropriate "flesh" to the "skeleton" we provide.

The initiator module describes BAX activation by BH3 proteins

When a stress signal is applied to the initiator module, the BH3 level increases. At first, these BH3 molecules are taken out of service by binding to inhibitory proteins (BCL2). If the stress signal is sustained, enough BH3 will accumulate to saturate the pool of antiapoptotic BCL2 molecules. Free, active BH3, we assume, induces conformational changes in BAX that facilitate its insertion into the mitochondrial outer membrane (24–26). The membrane-localized form of BAX (BAXm) binds strongly, we assume, to BCL2, releasing additional free BH3 to promote the conversion of BAX to BAXm.

To prevent cumulative activation of BAX to lethal levels by multiple, small, accidental activation events, there must be some protein(s) that inactivate BAX (BAXm $\rightarrow$ BAX) at a steady background rate. We assume that this inactivation process applies to bound forms of BAX (BAXm/BCL2 $\rightarrow$ BAX + BCL2) as well as to free forms. The alternative assumption that BAX inactivation only applies to the monomer form is invalid (see Appendix B for more details).

From a mathematical point of view, the initiator module exhibits bistability (alternative stable steady states of low and high BAX activity) when the inactivating enzyme works on BAXm/BCL2 as well as free BAXm, but the initiator module is monostable if the inactivating enzyme works on free BAXm only.

Bistability in the initiator module is central to our explanation of the signal threshold and time delay that are characteristic features of programmed cell death. Other authors have made different assumptions to generate bistable activation of BAXm (12,13), and further experimental investigations are needed to clarify the exact molecular mechanism.

In the model, we assume fixed total concentrations of BAX and BCL2. This assumption allows us to analyze the model by phase-plane techniques, as described later. Synthesis and degradation of BAX and BCL2 are incorporated later in the p53 model.

The amplifier module describes BAXm-induced release of CytoC and SMAC

Free BAXm causes an increase in mitochondrial outer membrane permeability (MOMP) (27). The exact mechanism of MOMP is not yet clear: BAXm proteins may form oligomers that perforate the membrane, or the outer membrane may swell and burst (28). In any case, we assume that BAXm forms tetramers that open channels in the mitochondrial outer membrane, as proposed in a previous model (7).

When channels are open (reaction CC $\rightarrow$ CO in Fig. 2 *B*), many different proapoptotic mitochondrial proteins can escape into the cytoplasm, including CytoC, SMAC, and apoptosis-inducing factor (AIF) (29). Among them all, SMAC and CytoC have been studied most intensively, and we focus on these two proteins in the current model. SMAC

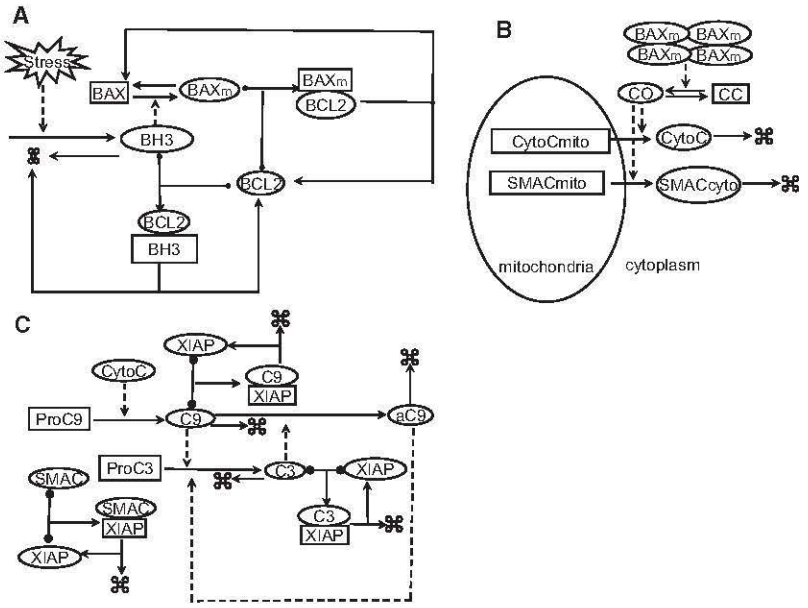

FIGURE 2 Wiring diagrams for a three-module decomposition of the intrinsic apoptotic pathway. (*A*) Initiator module. (*B*) Amplifier module. (*C*) Executioner module. Ovals and rectangles represent proteins in different activity states. Solid and dashed lines represent chemical reactions and regulatory signals, respectively. An arrow with two tails and one head represents the association of two proteins to form a complex. Black balls on the tails indicate a reversible association and dissociation reaction. An arrow with one tail and two heads indicates a complex that splits into two parts, with a chemical transformation (like degradation or inactivation) of at least one component. Five small circles represent degradation products. In *B*, the four BAXm icons represent a tetrameric complex that opens channels in the mitochondrial outer membrane. See text for details.

binds to and inhibits XIAP, an inhibitor of caspase 3 and caspase 9 (30,31), whereas CytoC activates caspase 9.

There are conflicting observations on whether executioner caspases feed back to BAX activation and CytoC release: some publications report that genetic knockout of caspases 3 and 7 affects CytoC release (32), whereas others report that inhibiting caspase activity does not affect BAX activation or mitochondrial release (33,34). Because of these inconsistencies, we do not incorporate feedback from caspases to the amplifier module.

The executioner module describes caspase activation by CytoC and SMAC

CytoC binds to APAF1 and to ATP (or dATP) to form trimers, APAF/ATP(dATP)/CytoC. Seven such trimers form an active apoptosome (29). The apoptosome recruits and activates caspase 9 (35) in the following manner. Caspase 9 is synthesized as inactive procaspase 9 (ProC9 in Fig. 2 *C*). Multiple procaspase 9 molecules bind to an apoptosome and cleave each other at the Asp^{315} residue (36). The cleavage products form a heterodimer, p35/p12 (C9 in Fig. 2 *C*). C9 is able to cleave procaspase 3 (ProC3) into active caspase 3 (C3) (29). Activated caspase 3 in turn cleaves C9 at Asp^{330}, creating a more active form, p35/p10 (aC9) (37). Caspase 3 may also cleave procaspase 9 to generate p37/p10 (37), but the physiological significance of this reaction is unclear, so we ignore it in the model.

Three forms of caspase 9 are considered in the executioner module: ProC9, C9 (p35/p12), and aC9 (p35/p10). CytoC causes ProC9 to become C9 and acquire basal protease activity; caspase 3 further cleaves C9 to generate a more active form, aC9. Since caspases function as homodimers, we use factors like $[C9]^2$ to describe caspase activity. Furthermore, since APAF1 and ATP (dATP) are readily available in the cytoplasm, we do not address the kinetics of apoptosome formation in the executioner module, although cooperativity of apoptosome assembly may have dynamical significance, as discussed elsewhere (10).

Stress-induced release of SMAC from mitochondria facilitates apoptosis by inhibiting XIAP, an inhibitor of executioner caspases. XIAP has a RING domain (30) and acts as an E3 ubiquitin ligase. It has been demonstrated that binding of XIAP to C3 (38) or SMAC (39) causes their polyubiquitination and degradation. XIAP also binds and inhibits C9, and we assume, in analogy to C3 and SMAC, that this binding leads to C9 degradation. However, XIAP does not bind to aC9, because the XIAP-binding site (four N-terminal amino acids of the p12 subunit) is removed when p12 is cleaved to p10 by C3 (40). Binding and dissociation of XIAP with caspase 3, caspase 9, and SMAC are all modeled explicitly, to take into account the competition of these proteins for XIAP.

Active caspase 3 (along with other executioner caspases) cleaves various substrates (4), causing multiple morphological changes, including chromatin condensation, nuclear shrinkage, DNA fragmentation, blebbing of the plasma membrane, and fragmentation of the cell. The executioner module uses caspase 3 activity as an indicator of cell death.

As outlined, there is strong positive feedback in the executioner module: C9 activates C3, which in turn changes C9 to aC9, a more active form of caspase 9 that is neither inhibited nor degraded by XIAP.

In response to DNA damage, p53 induces cell cycle arrest and apoptosis

p53 is a tumor suppressor protein: loss of p53 increases the chance of tumor development, whereas reactivating p53 has been proposed as a treatment for cancer (41). p53 suppresses tumor development by maintaining genome integrity in the face of DNA-damaging agents. When p53 is compromised,

cell lineages accumulate mutations that may lead ultimately to metastatic tumors.

In resting cells, the p53 level is kept low by a negative feedback through MDM2 (Fig. 3 *A*). Any accidental accumulation of p53 induces production of MDM2, which enhances p53 degradation. DNA damage disturbs the negative feedback by phosphorylating both p53 and MDM2. Phosphorylated p53 is more stable, and phosphorylated MDM2 is less active. DNA damage also enhances degradation of MDM2. By these effects, the p53 level is elevated in the presence of DNA damage (42–45).

p53 induces cell cycle arrest (in either G1 or G2) through transcriptional activation of p21, 14-3-3σ, and GADD45 (46). We focus on the well-studied pathway by which p53 induces synthesis of p21, which binds to and inhibits cyclin E-dependent kinase (Fig. 3 *D*). (We use "CDK" to refer to cyclin-dependent kinases in general and "CycE" to refer to the specific dimer of cyclin E and its catalytic subunit, Cdk2). p21 and CycE form an inactive complex. Since we do not know how complex formation affects the degradation of either p21 or CycE, we assume that both proteins can be degraded from the p21/CycE complex. As p21 is degraded, CycE is released and vice versa.

Lack of CDK activity leads to dephosphorylation of the retinoblastoma (RB) protein. Hypophosphorylated RB binds to and inhibits E2F1, a transcription factor needed for effective expression of cyclins E and A (47,48). Thus, if damage occurs in the G1 phase, CycE and CycA activities will drop precipitously, and the cell will not progress into the S phase (DNA synthesis). If DNA damage occurs later in the cycle, a low level of CycA and a high level of p21 will prevent accumulation of CycB activity, which is necessary for the cell to enter mitosis.

p53 triggers apoptosis in multiple ways (22,23), the best characterized of which is transcriptional activation of BH3 proteins (Fig. 3 *C*), including BID, BIM, PUMA, and NOXA (46,49). We divide these BH3 proteins into two different classes, BH3AC and BH3DR. BH3AC (representing BID and BIM) both binds to BCL2 proteins and activates BAX directly. BH3DR (representing PUMA and NOXA) only binds to BCL2 proteins.

p53 induces other proapoptotic proteins, e.g., Fas, DR5, PIG3, IGF-BP3, p53AIP1, and PTEN. These proteins are beyond the scope of this model, but they may be included in future extensions. p53 also induces BAX and APAF1; however, their induction seems not essential, since active BH3 proteins are able to trigger mitochondrial permeability and apoptosis even when protein synthesis is blocked with cycloheximide (7).

E2F1 enhances apoptosis

E2F1 participates in p53-induced apoptosis in several ways (Fig. 3 *A*) (50,51). E2F1-induced ARF inhibits MDM2, thereby promoting p53 accumulation (45). E2F1 also induces ASPP1 and 2, JMY, and p53DINP1 (modeled collectively as ASPP in Fig. 3); these cofactors enhance the efficiency of p53 in inducing proapoptotic target genes. E2F1 also contributes to apoptosis independently of p53 by inducing p73, a transcription factor in the same family as p53 (52).

Furthermore, E2F1 binds to p53 and retains it in the nucleus (53). E2F1 also induces APAF-1 and other apoptosis regulators (51,54,55), but we choose not to include these regulations in this model.

Differentially modified p53 can be divided into "helper" and "killer" classes

p53 function is modulated by extensive posttranslational modifications, including phosphorylation, methylation, acetylation, and ubiquitination (46,56,57). In addition, various

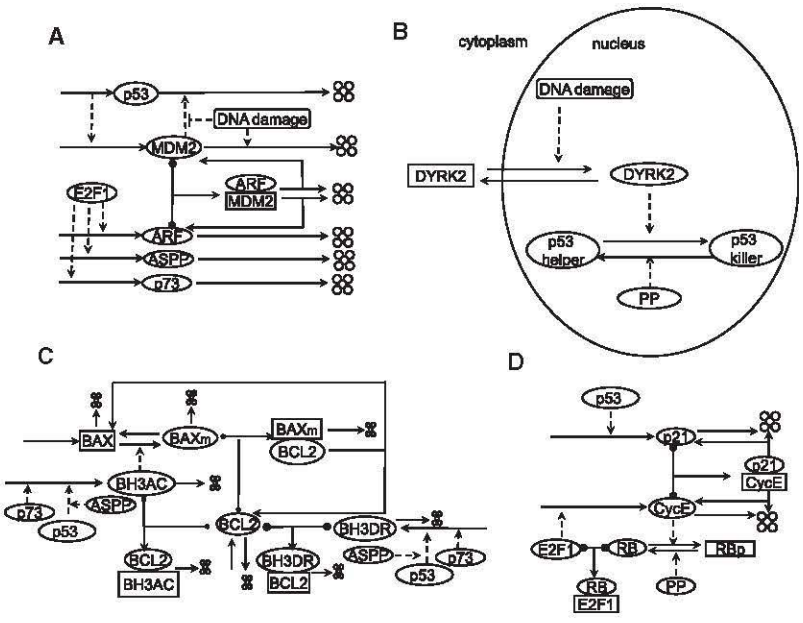

FIGURE 3 Wiring diagrams for processes regulating p53 and those regulated by p53. (*A*) E2F1 enhances apoptosis. (*B*) DYRK2 transforms p53 helper to p53 killer. (*C*) p53 and p73 induce apoptosis. (*D*) p53 inactivates E2F1. Notations are as in Fig. 2. See text for details.

cofactors (e.g., ASPP1/2, HZF, and BRN3) bind to p53 and direct it to specific target genes (58). p53 modifications affect its binding to certain cofactors and vice versa (53,56).

In our model, we assume that posttranslation modification and cofactor-binding result in two types of p53: one type prefers the induction of apoptosis and the other prefers the induction of cell cycle arrest (58). We name the proapoptotic type "p53 killer" and the proarrest type "p53 helper" (Fig. 3 *B*). In the model, we take Ser^{46} phosphorylation as an exemplar of the killer class. When more data on other forms of modification and cofactor binding are available, the model can be extended to more subtle distinctions among p53 functional classes.

A dual-specificity tyrosine-phosphorylation-regulated kinase (DYRK2) is cytoplasmic in resting cells but translocates to the nucleus after DNA damage (58), where it phosphorylates p53 on Ser^{46}. When DYRK2 is knocked down with siRNA, DNA-damage-induced apoptosis is impaired (59). In the model, p53 accumulates initially in the helper form, and later it is converted into the killer form by DYRK2.

METHODS

A mathematical model (Appendix A) has been constructed from the proposed molecular mechanisms in Figs. 2 and 3 by standard principles of biochemical kinetics, as practiced in Tyson's research group (60,61). The mechanisms are based on our review of the experimental literature, as outlined in the section "Model assumptions and molecular justifications". Some assumptions have been made to fill gaps in the available evidence. The proposed mechanism focuses attention on the molecular components and reactions that we believe are crucial to understanding apoptotic decision-making. The time-dependent variables of the model are summarized in Table 1. Other relevant proteins, not explicitly modeled, are listed in Table 2.

Time is expressed in minutes, so all rate constants have units min^{-1}. All "concentrations" are expressed in "arbitrary units" (i.e., they are dimensionless). Dimensionless concentrations are used because we do not have enough experimental data to confidently estimate intracellular concentrations of all proteins in the model, and because some variables, such as [BH3] and [BCL2], represent combinations of several proteins. Values for the rate constants were chosen by trial and error, to give simulations and bifurcation diagrams that are consistent with known properties of programmed cell death. Interested readers can consult previous models for more information on the rate constants (10,12–14,17–19,62).

We analyze the differential equations with standard tools of dynamical systems theory (phase-plane analysis and bifurcation theory), and we simulate their solutions numerically with standard algorithms for stiff ordinary differential equations (ODEs). The software tools we prefer are XPP-AUT (http://www.math.pitt.edu/~bard/xpp/xpp.html) and Oscill8 (http://oscill8.sourceforge.net/). In the online Supporting Material, we provide "ode" files for studying our models with these tools. Ode files are easily adapted to other software environments like MATLAB or Madonna.

RESULTS

The initiator module is responsible for the threshold and time-delay properties of apoptosis

The initiator module (Fig. 2 *A*) can be described by four ODEs (Appendix A), once we assume constant total concentrations of BAX and BCL2 proteins ($[\text{BAX}]_\text{T}$ and $[\text{BCL2}]_\text{T}$). All numerical simulations and bifurcation calculations are done on these four ODEs. However, to gain insight into the dynamics of the initiator module, it is useful and convenient to write the four ODEs as a pair of differential equations for the "slow" variables, $[\text{BH3}]_\text{T} = [\text{BH3}]_\text{F} + [\text{BH3/BCL2}]$, and $[\text{BAXm}]_\text{T} = [\text{BAXm}]_\text{F} + [\text{BAXm/BCL2}]$, where the subscript "F" indicates the "free" proteins not bound to BCL2:

$$\frac{d[\text{BAXm}]_\text{T}}{dt} = \left(k_{f1} + k_{f2} \times [\text{BH3}]\right) \times [\text{BAX}] - k_b \times [\text{BAXm}]_\text{T}, \tag{1a}$$

$$\frac{d[\text{BH3}]_\text{T}}{dt} = k'_{\text{sBH3}} + k''_{\text{sBH3}} \times \text{Stress} - k_{\text{dBH3}} \times [\text{BH3}]_\text{T}, \tag{1b}$$

and a pair of algebraic equations for the steady-state concentrations of protein complexes,

$$K_1[\text{BH3/BCL2}] = \left([\text{BH3}]_\text{T} - [\text{BH3/BCL2}]\right) \times \left([\text{BCL2}]_\text{T} - [\text{BH3/BCL2}] - [\text{BAXm/BCL2}]\right), \tag{2a}$$

$$K_2[\text{BAXm/BCL2}] = \left([\text{BAXm}]_\text{T} - [\text{BAXm/BCL2}]\right) \times \left([\text{BCL2}]_\text{T} - [\text{BH3/BCL2}] - [\text{BAXm/BCL2}]\right), \tag{2b}$$

where $K_1 = \dfrac{k_{\text{dsBH3BCL2}} + k_{\text{dBH3}}}{k_{\text{asBH3BCL2}}}$, $K_2 = \dfrac{k_{\text{dsBAXmBCL2}} + k_b}{k_{\text{asBAXmBCL2}}}$. By formulating the initiator module in this way, we can study its dynamics using phase-plane methods (Fig. 4 *A*). The balance curve (also called a "nullcline") for $[\text{BH3}]_\text{T}$ is a vertical line according to Eq. 1b. Stress enhances the synthesis of BH3 and moves the $[\text{BH3}]_\text{T}$ balance curve to the right. The balance curve for $[\text{BAXm}]_\text{T}$ is S-shaped because of positive feedback in the initiator module, to be described below.

Wherever the balance curves intersect, the system attains a steady state. For a small stress signal (Stress = 0.1), the system has one steady state with a low level of BH3 proteins ($[\text{BH3}]_\text{T} = 16$) and negligible $[\text{BAXm}]_\text{F}$ (since all BAXm proteins bind to BCL2 proteins). This steady state (on the lower branch of the S-curve) corresponds to living cells. The living state is robust, in the sense that small fluctuations of BAXm or BH3 levels will decay over time, as the control system returns to the stable steady state. For a large enough stress signal (e.g., Stress = 0.6), the BH3 balance curve intersects only with the upper branch of the S-curve. Now the living state is lost, and the system moves to a steady state of high $[\text{BAXm}]_\text{F}$ (the apoptotic state).

The life-to-death transition occurs when BCL2 is titrated out by BAXm and BH3, such that $[\text{BCL2}]_\text{T} \approx [\text{BAXm}]_\text{T} + [\text{BH3}]_\text{T}$. Given the parameter settings in Appendix A, the steady state of the initiator module at rest (for Stress = 0.1) is $[\text{BH3}]_\text{T} \approx [\text{BH3/BCL2}] \approx 16$, $[\text{BAXm}]_\text{T} \approx [\text{BAXm/BCL2}] \approx 33$, and $[\text{BCL2}]_\text{F} \approx 31$. Hence, $[\text{BH3}]_\text{T}$ must attain a value of ~47 to titrate out all the remaining BCL2

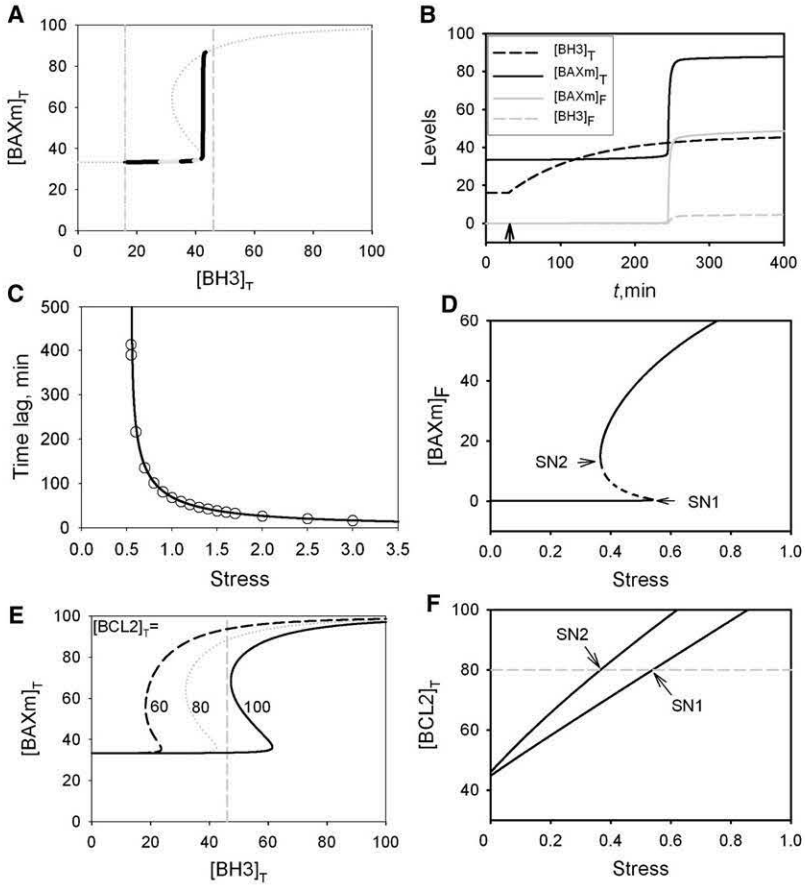

FIGURE 4 Analysis of the dynamics of the initiator module. (*A*) Phase plane. *Gray dotted line*, balance curve for $[BAXm]_T$; *gray vertical lines*, balance curves for $[BH3]_T$ (*dash dotted*, Stress = 0.1; *dashed*, Stress = 0.6); *black-gray solid line*, life-to-death trajectory followed by $[BH3]_T$ and $[BAXm]_T$, plotted as time series in *B*. Dashes change color between black and gray every 50 min after the stress signal is applied. (*B*) The time series of $[BH3]_T$, $[BAXm]_T$, $[BAXm]_F$, and $[BH3]_F$. Stress = 0.1 for $t < 30$ and 0.6 for $t > 30$. The black arrow here and later indicates the time of application of stress. (*C*) Time lags between stimulation and BAXm activation for different values of stress. *Open circles*, time lags from model simulations; *solid line*, time lag predicted by Eq. 3. (*D*) One-parameter bifurcation diagram. Solid and dashed lines correspond to stable and unstable steady states, respectively. (*E*) Phase plane for three different values of $[BCL2]_T$. *Gray dashed line*, $[BH3]_T$ balance curve for Stress = 0.6; *black dashed*, *gray dotted*, and *black solid lines*, $[BAXm]_T$ balance curves for $[BCL2]_T = 60$, 80, and 100, respectively. (*F*) Two-parameter bifurcation diagram. *Black solid lines*, saddle-node bifurcation points; *gray dashed line*, corresponds to one-parameter bifurcation shown in *D*. The region of bistability is between the black solid lines.

molecules. This estimate differs from the calculated threshold of 43 because the binding of BCL2 to BAXm and BH3 is not infinitely strong.

To study the dynamics of the transition, we first let the system evolve to the living state with a small stress signal (0.1) and then increase the stress signal to 0.6. At the high stress level, the system starts producing lots of BH3 protein. At first, most BH3 molecules bind with BCL2, so they cannot activate BAX. Eventually, BH3 titrates out the BCL2 pool, and excess BH3 molecules are now free to convert BAX to BAXm. BAXm displaces additional BH3 from the BH3/BCL2 dimer pool, thereby speeding up its own production from inactive BAX. This positive feedback causes the BAXm level to rise quickly, which will be sufficient to activate the amplifier module (Fig. 4 *B*). The trajectory is plotted on the $[BAXm]_T$-$[BH3]_T$ plane (Fig. 4 *A*). In the final phase of the initiator module, the system moves along the top branch of the BAXm balance curve, approaching asymptotically to the steady state.

Note that since $[BAXm]_T$ changes much faster than $[BH3]_T$, the trajectory approaches the $[BAXm]_T$ balance curve quickly, and the life-to-death transition is driven by the accumulation of BH3 proteins. As $[BH3]_T$ approaches the vertical balance curve (where $d[BH3]_T/dt = 0$), the rate by which $[BH3]_T$ increases gets smaller. Hence, the location of the vertical nullcline, at $[BH3]_T = (k'_{sBH3} + k''_{sBH3} \times \text{Stress})/k_{dBH3}$, determines the time needed for the life-to-death transition. For example, for Stress = 0.6, the vertical balance curve (at $[BH3]_T = 46$) is barely above the threshold (~43), so it takes a long time to make the transition. As stress increases, the vertical balance curve moves to the right, and $[BH3]_T$ can increase more quickly toward the threshold. This effect explains the observed inverse relationship between signal strength and time lag for initiation of apoptosis (7). This phenomenon is called "critical slowing down" in bifurcation theory.

From Eq. 1a, it is easy to derive an analytical approximation for the lag time, T_L,

$$T_L \approx \frac{1}{k_{dBH3}} \ln\left(\frac{[BH3]_T^{\infty} - [BH3]_T^{0}}{[BH3]_T^{\infty} - [BH3]_T^{\theta}}\right), \quad (3)$$

where $[BH3]_T^0 = \dfrac{k'_{sBH3} + 0.1 \times k''_{sBH3}}{k_{dBH3}}$ is the initial concentration of BH3 at the resting state (Stress = 0.1), $[BH3]_T^{\infty} = \dfrac{k'_{sBH3} + k''_{sBH3} \times \text{Stress}}{k_{dBH3}}$ is the final concentration of BH3, and $[BH3]_T^{\theta} = 43$ is the threshold concentration of BH3. In Fig. 4 *C*, we compare the analytical approximation (3) with the computed lag time as a function of stress.

Bifurcation theory provides an accurate analysis of how the activation threshold depends on stress and $[BCL2]_T$. In the one-parameter bifurcation diagram (Fig. 4 *D*), we plot the steady-state level of $[BAXm]_F$ as a function of stress. For

low stress, the system shows one stable steady state with $[BAXm]_F \approx 0$. As stress increases, this stable steady state is lost at a saddle-node bifurcation point (SN1). Beyond the bifurcation point, the system moves to a stable steady state with high $[BAXm]_F$. The saddle-node bifurcation point corresponds to the threshold level of stress necessary to fire the initiation module. If stress is reduced after the module has fired, then the high $[BAXm]_F$ state persists until stress drops below a different, lower threshold (corresponding to SN2 in Fig. 4 *D*).

Changing $[BCL2]_T$ modulates the threshold stress signal that activates BAXm. The effect is demonstrated on the phase plane (Fig. 4 *E*) and then captured in a two-parameter bifurcation diagram (Fig. 4 *F*). The two lines in this figure trace the positions of the two saddle-node bifurcations (Fig. 4 *D*, *SN1* and *SN2*) with changing levels of total BCL2. The two-parameter plane is divided into three regions by the saddle-node lines: the region to the left of SN2 (low stress, high $[BCL2]_T$, and low $[BAXm]_F$) corresponds to the living state; the region to the right of SN1 (high stress, low $[BCL2]_T$, and high $[BAXm]_F$) corresponds to the apoptotic state; and the region between the SN lines is the bistability zone. The saddle-node line separating the bistable region from the apoptotic region determines the threshold stress level for the initiator module to fire. Clearly the threshold increases linearly with $[BCL2]_T$, in agreement with the idea that apoptosis is induced when BCL2 is titrated out.

The amplifier module describes CytoC and SMAC release

As $[BAXm]_F$ increases, oligomers form and open channels in the mitochondrial outer membrane. CytoC and SMAC leave mitochondria through these channels and enter the cytoplasm, where they cooperate to activate the executioner caspase 3 and then eventually get degraded. Given the parameter settings in our model, the amplifier module merely relays the signal from BAX in mitochondria to caspases in the cytoplasm. The all-or-none accumulation of active BAX in mitochondria membrane results in an all-or-none release of CytoC and SMAC, which has been observed (7,63).

The executioner module is responsible for committed cell death

To characterize the executioner module, we use bifurcation diagrams again. In Fig. 5 *A*, we plot steady-state caspase 3 activity as a function of [CytoC] for fixed $[SMACcyto]_T = 2$. It is clear that the executioner module exhibits bistability and hysteresis, after we have chosen suitable parameter values for the assumed positive feedback between caspase 9 and caspase 3.

Since CytoC and SMAC are released together when mitochondrial channels open, it is natural to use a two-parameter bifurcation diagram (Fig. 5 *B*) to show how caspase 3 activation depends on simultaneous variations of both proteins. The cusp-shaped region in this diagram is the region of bistability. The rightmost saddle-node line is the threshold for caspase 3 activation. A resting cell starts out in the "living" zone with $[SMACcyto]_T \approx 0$ and $[CytoC] \approx 0$ and low caspase 3 activity (Fig. 5 *B*, position 1). As CytoC and SMAC are released from mitochondria in response to stress, the cell progresses along the black solid line toward the apoptotic transition (position 2). Once caspase 3 is activated, it stays active until degradation of CytoC and SMAC drives the system back toward the "living" zone (caspase 3 inactivation occurs at position 3).

To compute bifurcation diagrams (with steady-state levels of active caspase 3), we are compelled to assume constant levels of total caspase 3 and total caspase 9 and use them as parameters. This assumption is not correct; rather, the cell possesses initial supplies of procaspase 3 and procaspase 9, supplies that are used up as the cell executes the death

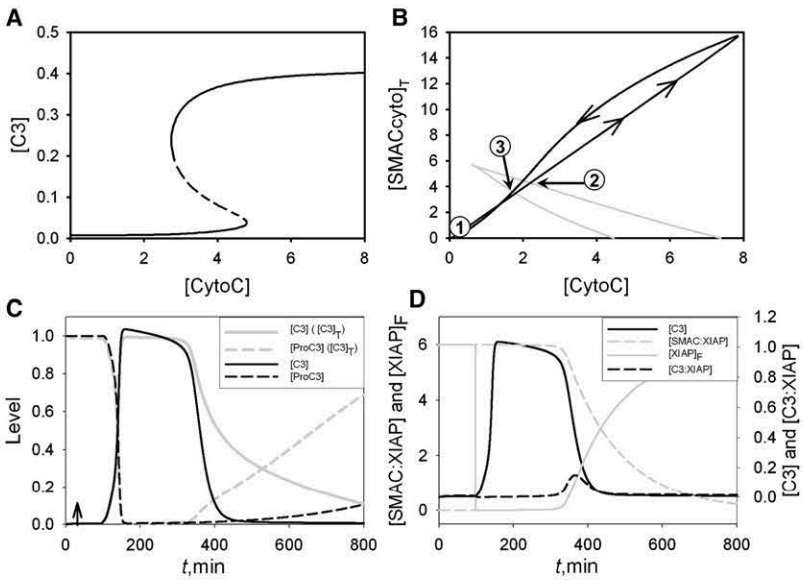

FIGURE 5 Bifurcation diagrams for the executioner module. (*A*) One-parameter bifurcation diagram (steady-state C3 activity as a function of CytoC) for $[SMACcyto]_T = 2$. Notations are as in Fig. 4 *D*. (*B*) Two-parameter bifurcation diagram. *Gray lines*, loci of saddle-node bifurcations; *black line*, trajectory of CytoC and $[SMACcyto]_T$ in the cytoplasm as apoptosis is executed. See text for more details. (*C*) Comparison of time courses. Gray lines are computed with constant total caspase 3 and total caspase 9; black lines are computed after incorporating synthesis and degradation of the caspases. See text for more details. (*D*) Elevated caspase 3 activity is maintained by SMAC-inhibition of XIAP. See text for details. The time-course simulations in *B–D* are computed with the complete apoptosis model: Stress = 0.1 for $t < 30$ and 1 for $t > 30$.

program. However, time-course simulations (Fig. 5 *C*), in which we incorporate the synthesis and degradation of procaspase 3 and procaspase 9, show that the assumption of constant total procaspases is a good approximation for the first few hours. Hence, the insights provided by the bifurcation diagrams are valid for the early stage of apoptosis.

From the time-course simulations in (Fig. 5 *C*), we see that procaspase 3 is quickly consumed once apoptosis is triggered, which means that inflow to the pool of procaspase 3 is very low. The only way to maintain a high level of caspase 3 in cells is to shut down the degradation of caspase 3 by XIAP, which is the function of SMAC (Fig. 5 *D*). When SMAC is released into the cytoplasm, it sequesters XIAP. As long as there is enough SMAC to block XIAP action, caspase 3 stays at a high level. Later, since SMAC itself is subject to XIAP-induced degradation, SMAC level drops below the level of XIAP, and then free XIAP causes degradation of caspase 3. In a word, excess SMAC protein is important for sustained caspase 3 activity and committed cell death through the intrinsic apoptosis pathway.

The model captures the dynamic features of normal apoptosis

After analyzing each module separately, we put them together to simulate the progression of apoptosis in wild-type cells. We start the simulation from the resting state (Stress = 0.1) and elevate the stress signal to different levels at $t = 30$. Model simulations (Fig. 6 *A*) exhibit the three characteristic features of apoptosis (7,18,64):

1. BAXm and caspase 3 are activated only when stress exceeds a certain threshold (~0.5 for the parameter values used here). The threshold property protects cells from unexpected fluctuations in stress.
2. In response to suprathreshold stress signals, there is a distinct time lag before caspase 3 is activated. As stress increases, the time lag decreases. However, neither the amplitude nor the duration of caspase 3 activity is sensitive to the level of stress above the threshold. The time delay gives cells some time before making the final commitment to apoptosis. If the stress signal disappears soon, cells may survive.
3. Once caspase 3 is activated, its activity stays high for a certain period of time, ensuring that the apoptotic process is carried to completion. This commitment feature is essential to prevent cells that have been damaged by apoptotic DNases from reverting to a proliferative state and propagating their damaged DNA to progeny cells.

The sequential activation of BAXm and caspase 3 agrees with experimental observations. When increasing levels of death ligand (like TRAIL) are used to induced apoptosis, decreasing time lags are observed before MOMP, but caspase 3 activation after MOMP is always quick (7,18).

Cells have good reason to control apoptosis upstream of BAX activation. Mitochondria generate most of the cell's energy supply, so it makes sense not to permeabilize the mitochondrial outer membrane before the cell determines to self-destruct. Release of other mitochondrial proteins may cause considerable caspase-independent damage (65).

Now we take a closer look at the events between MOMP and caspase 3 activation (Fig. 6 *B*). SMAC is released into the cytoplasm, where it binds to XIAP and reduces the pool of free inhibitors. At the same time, caspase 9 is activated by cytoplasmic CytoC. Caspase 9 is free to activate caspase 3, since there is no XIAP to inhibit caspases 3 and 9. Caspase 3 then converts caspase 9 into a more active form, bringing about an explosive increase in caspase 3 activity. Caspase 3 activity stays high until SMAC level is greatly reduced and no longer able to hold XIAP inactive. Prolonged caspase 3 activity, which has been observed experimentally (64,66), ensures complete cleavage of its cellular substrates.

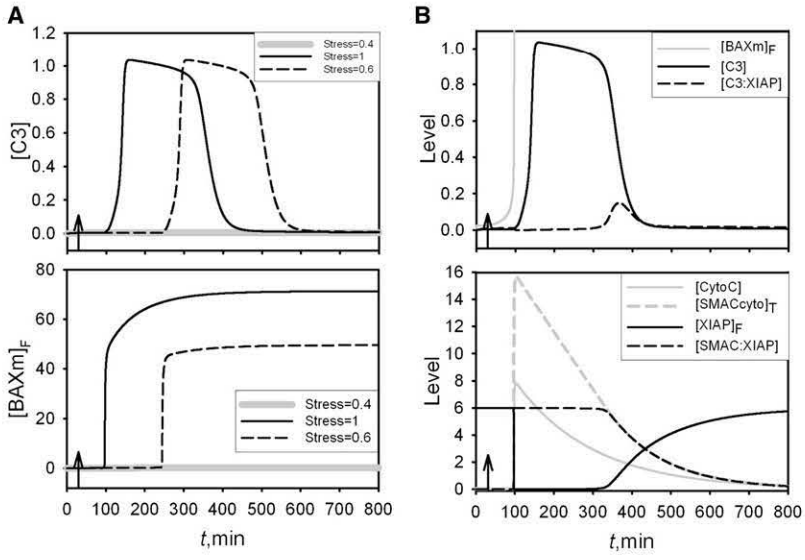

FIGURE 6 Simulated protein time courses demonstrating how the model captures the dynamical features of a normal apoptotic response. (*A*) Caspase 3 activity and free BAXm level. For $0 < t < 30$, Stress = 0.1, and for $t > 30$, stress is raised to different levels. (*B*) Time courses of other proteins for the case Stress = 1 for $t > 30$.

In the model, caspase 3 inactivation occurs after SMAC is degraded enough to release XIAP. Since the cell is already "dead" by this time, caspase inactivation in the model is a moot point. However, if SMAC protein level is low or XIAP protein level is high, the executioner module may allow for premature inactivation of caspase 3. Cells compromised in this fashion have the potential to develop into tumors. The loss of commitment in mutant cells will be addressed in more detail later.

The model mimics the dynamics of apoptosis in mutants and provides mechanistic insights

We test the model by examining its ability to simulate mutant phenotypes. To simulate a mutant cell line, we change the values of appropriate parameters in the model. To mimic XIAP overexpression or deficiency mutants, we change $[XIAP]_T$ from its wild-type value of 6 to 13 or 1, respectively. To mimic cells with double deficiency of BID and BIM, we change k_{f2} to zero. We start each mutant simulation from the resting state, Stress = 0.1, and then set Stress = 1 at $t = 30$.

Caspase 3 activity and free BAXm level in wild-type and double-deficient cells are plotted in Fig. 7 *A*. In wild-type cells, caspase 3 is activated after a lag of ~70 min and stays active for another 250 min. In cells deficient for BID and BIM ($k_{f2} = 0$), there is a slightly longer time delay, but caspase 3 activity is eventually high enough and sufficiently sustained to commit the cell to death, as observed experimentally (67).

The time course of free BAXm level reveals a defect in BAX activation when BID and BIM are knocked out; however, this malfunction of the initiator module is not seen as a significant defect in the apoptotic response, because the amplifier module and executioner module can still turn a graded response of BAXm into a committed response of caspase 3 activity. To observe the consequences of the mutation would require closer examination of BAX dynamics in the mitochondria. We propose below an experiment to achieve this.

Caspase 3 activities in wild-type and mutant cells with two different levels of XIAP are plotted in Fig. 7 *B*. In XIAP-deficient mutants ($[XIAP]_T = 1$), caspase 3 is activated as in wild-type cells, but caspase 3 activity stays high for a longer time. Hence, XIAP-deficient cells are surprisingly normal (68); they respond properly to small and large stress signals. The normal behavior of XIAP-deficient cells is due to a functional compensation of the defect by the initiator module.

On the other hand, when XIAP is over-expressed ($[XIAP]_T = 13$), caspase 3 is activated only transiently, which is consistent with the observation of partial caspase 3 activation in XIAP overexpressing cells (18). In this case (Fig. 7 *C*), as SMAC is first released from mitochondria, it inhibits XIAP and allows caspase 3 activation. However, SMAC soon loses its control over XIAP, since the XIAP level is high. Free XIAP binds to caspase 3 and causes its degradation. Thus, caspase 3 stays active for only a short period of time.

The p53 module governs dynamical cell fates after DNA damage

In this section, we use bifurcation diagrams to study the p53 signaling module (Fig. 3). First, we take p53 "helper" and "killer" activities to be fixed parameters and examine the response of the system in terms of E2F1 activity and BAX activation. (Since, as we have shown, BAX activation by the initiator module is sufficient to trigger apoptosis in wild-type cells, we need not trace the process beyond BAXm). In Fig. 8 *A*, we set p53 killer to the low level of 1 and plot steady-state E2F1 activity as a function of the p53-helper level. At low p53-helper level, E2F1 activity stays high, corresponding to proliferating cells. As the p53-helper level increases, E2F1 becomes inactived by RB (see Fig. 3 *D*), resulting in cell cycle arrest. The high E2F1 state is lost by

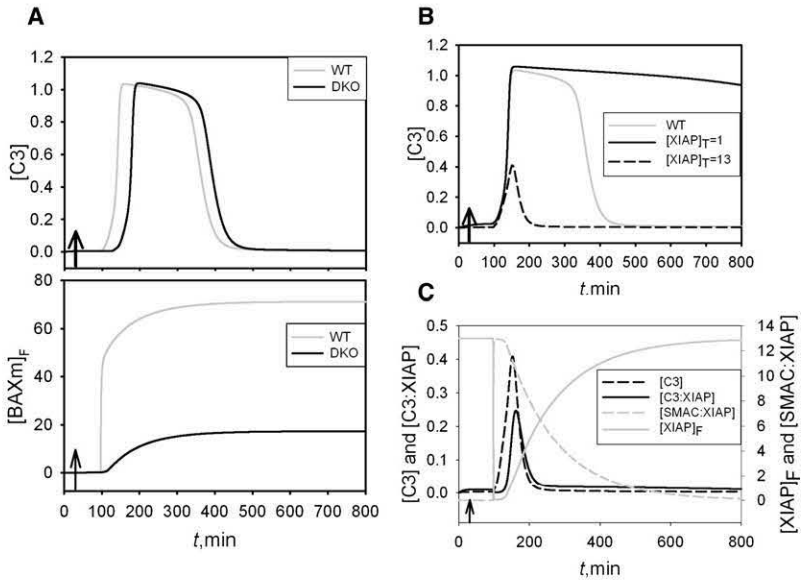

FIGURE 7 Comparisons of time courses for wild-type and mutant cells. (*A*) Time course of C3 activity, as well as free [BAXm] level for wild-type cells and the double knock-out mutant ($bid^{-/-}$ $bim^{-/-}$; $k_{f2} = 0$). Stress is raised from 0.1 to 1 at $t = 30$. (*B*) Time course of C3 activity for wild-type and two different levels of $[XIAP]_T$. (*C*) Loss of commitment for cells overexpressing XIAP. See text for more details.

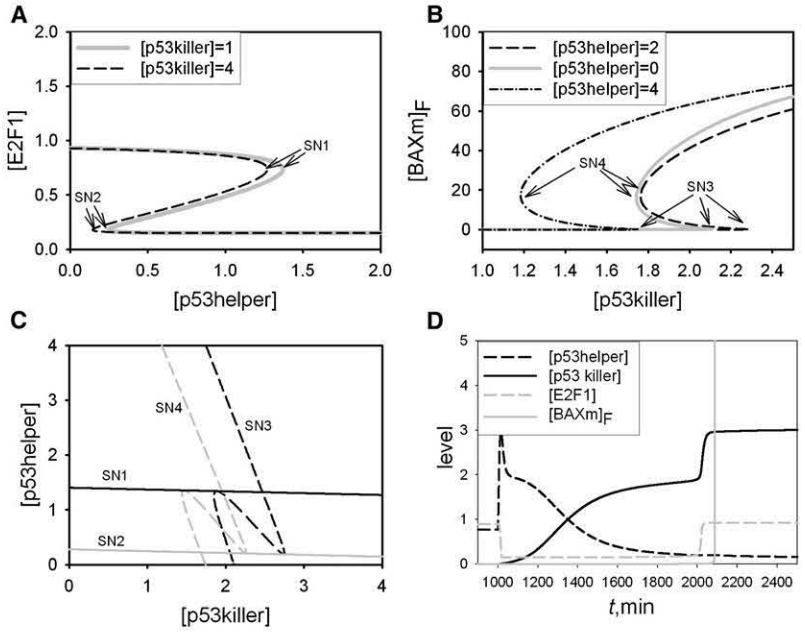

FIGURE 8 The transformation from p53 helper to p53 killer in response to prolonged DNA damage. (*A*) E2F1 inactivation by p53 helper: one-parameter bifurcation diagrams for two different levels of p53 killer. (*B*) BAXm activation by p53 killer: one-parameter bifurcation diagrams for three different levels of p53 helper. For *A* and *B*, there are three steady states between the saddle-node (SN) bifurcations; the middle state is unstable. (*C*) Two-parameter bifurcation diagram for p53 killer and p53 helper. Solid and dashed lines trace saddle-node bifurcations in *A* and *B*, respectively. (*D*) Dynamical cell fate in response to DNA damage. DNA damage = 0 for $0 < t < 1000$, and DNA damage = 10 for $t > 1000$.

a saddle-node bifurcation, due to the positive feedback between CycE and E2F1 (CycE/Cdk ⊣ RB ⊣ E2F1 → CycE). When p53 killer is increased (to 4), a little less p53 helper is needed to inactivate E2F1, but the effect is inconsequential (SN1 shifts only slightly), because the ability of p53 killer to induce p21 is assumed to be very small.

Next, we set p53 helper to 0 and investigate the p53-killer effect (Fig. 8 *B*). At a low level of p53 killer, $[BAXm]_F$ stays low. As p53-killer level increases, BH3 proteins are introduced. At first, there is enough BCL2 to sequester all BAXm and BH3 molecules, and $[BAXm]_F$ remains low. As the p53-killer level passes a certain threshold, BCL2 proteins are titrated out and the positive feedback between BAXm and BH3 brings a sudden increase of active BAXm molecules (at SN3), causing MOMP and caspase 3 activation, as described earlier.

Increasing the p53-helper level shows dual effects on p53-killer-induced apoptosis (Fig. 8 *B*). When p53 helper is increased a little (p53 helper = 2), apoptosis is inhibited: a little more p53 killer is required to activate BAXm. However, further increase, to p53 helper = 4, promotes apoptosis with considerably less p53 killer needed to activate BAXm (the position of SN3 drops significantly).

A two-parameter bifurcation diagram (Fig. 8 *C*) lays out the interactions between p53 helper and p53 killer. In this diagram, solid lines trace the pair of saddle-node bifurcation points (*black*, SN1; *gray*, SN2) by which p53 helper induces cell cycle arrest, and dashed lines trace the pair of saddle-node bifurcation points by which p53 killer induces apoptosis (*black*, SN3; *gray*, SN4). The solid lines are nearly horizontal, in agreement with the fact that p53 killer hardly affects p53-helper-induced cell cycle arrest.

The dashed lines have two features. First, they move leftward with increasing p53 helper. Because p53 helper contributes to the production of BH3 proteins, increasing the p53-helper level promotes the induction of apoptosis by p53 killer. Second, the dashed lines are N-shaped, which reflects the saddle-node bifurcations observed in Fig. 8 *A*. For a low level of p53 helper (below the line for SN2), E2F1 is active and enhances p53-induced apoptosis (see Fig. 3 for the molecular mechanism); hence, the p53 killer level needed to induce apoptosis is low. When p53 helper level is increased above the line for SN1, E2F1 is inhibited and unable to promote apoptosis; thus, the threshold level of p53 killer is elevated abruptly. Positive feedback in E2F1 regulation (described above) is necessary for bistability observed in Fig. 8 *A* and the N-shaped bifurcation curves in Fig. 8 *C*.

Between the lines for SN1 and SN2, the bifurcation analysis becomes more complicated and beyond the scope of this manuscript.

Now that we know the different functions of p53 helper and p53 killer, we can investigate how these two forms are regulated in response to DNA damage (Fig. 8 *D*), using the ODEs for the p53 module in Appendix A. In the absence of DNA damage, the equations reach a steady state, corresponding to resting cells. As a damage signal is applied, [MDM2] decreases and [p53] increases. At first, p53 accumulates in the helper form; cell cycle progression is arrested and apoptosis is inhibited. If the damage is repaired quickly, the cell may go back to proliferation. Sustained DNA damage, on the other hand, causes DYRK2 translocation to the nucleus, where it transforms p53 helper to p53 killer. p53 killer induces BH3 proteins more efficiently than p53 helper. Furthermore, E2F1 is reactivated as the p53 helper level decreases, and active E2F1 helps p53 to induce apoptosis.

Experimental observations support the dynamical changes proposed by the model. For example, when p53 is activated by DNA damage, the cell cycle arrest protein p21 is induced earlier than the apoptotic protein PUMA (69).

DISCUSSION

Programmed cell death (apoptosis) has three defining dynamical features: a signal threshold that must be exceeded to elicit cell death, a long and variable time delay between the signal and the response, and irreversible commitment to cellular disassembly once the terminal proteases have been activated. From the available experimental data we have identified those molecular interactions that, we believe, are key components of the mechanisms ensuring these properties of programmed cell death. Using a mathematical model, we show how the dynamical features arise from the identified interactions. The model attributes the signal threshold and time delay to positive feedback between proapoptotic BH3 and BAX proteins mediated by antiapoptotic BCL2 proteins. Activated BAX proteins release cytochrome *c* and SMAC from mitochondria, and these signaling proteins stimulate a positive feedback between caspase 9 and caspase 3 that ensures irreversible commitment to cell dissolution. As an example of how this cell-death response network responds to stress signals, we propose a model of how p53 responds to DNA damage by eliciting, at first, cell cycle arrest and damage repair, and later, if the damage persists, cell death. The sequence of protein expressions and posttranslational modifications, generated by the model, are in qualitative agreement with experimental observations.

Several other studies using computational modeling to understand the molecular machinery underlying apoptosis have been published in recent years. Each model has its own unique scope and emphasis. Our model has been designed to combine what we believe are the best characteristics of previous modeling efforts with some novel ideas and specific goals of our own.

We are interested in how cells respond to severe DNA damage by cell cycle arrest and, ultimately, programmed cell death. Hence, we choose to emphasize the role of BH3 proteins in sensing the damage signal. By contrast, Albeck et al. (7,19) are interested in how apoptosis is stimulated by external signaling factors, so their model starts from the binding of a death ligand to its membrane receptor. Their model is concerned with, among other things, interactions between the extrinsic and intrinsic pathways of apoptosis. The model by Rehm et al. (18) starts from mitochondrial release of CytoC and SMAC, to focus on the role of XIAP in caspase 3 activation.

We are particularly interested in the molecular mechanisms that underlie the threshold, time-lag, and commitment properties of apoptosis, which leads us to select some molecular interactions for our model and disregard others. The biochemical details we have disregarded may prove important in addressing other issues. For example, we do not model apoptosome assembly explicitly, but this process plays an important role in the model of Bagci et al. (10), who attribute bistability in caspase 3 activation to cooperativity in apoptosome formation (Apaf1 + CytoC + caspase 9 + ATP $\rightarrow$ Apoptosome) and feedback from caspase activation to CytoC release from mitochondria. In addition, we disregard the feedback from caspase 3 to caspase 8 through caspase 6, but this positive feedback loop plays a significant role in the model of Eissing et al. (14), generating bistability in caspase 3 activation.

The final stage of programmed cell death is a transient disassembly of the cell (a dying cell is certainly not at a steady state). However, preliminary stages of the process have time to reach a pseudosteady state before final activation of executioner caspases. Furthermore, an analysis of steady states of the several stages of programmed cell death is very informative about the transient behavior of the control system, as we have shown. Hence, we use bifurcation diagrams extensively to reveal how qualitative features of the apoptotic response are related to network motifs in the reaction mechanism and to quantitative aspects of the network, such as gene expression levels and kinetic rate constant changes induced by mutations. By contrast, Albeck et al. (7,19) are interested in comparing their model with experimental observations, so they rely heavily on numerical simulations. To capture the stochastic effects in the apoptotic response, Chen et al. (12) use agent-based simulations to study their model's predictions. Stochastic effects in apoptosis have also been addressed by Eissing et al. (14,62).

Our emphasis on positive feedback, bistability, thresholds, and time lags is based in part on previous studies of programmed cell death. Legewie et al. (17) have studied two possible positive feedback loops between caspase 3 and caspase 9, and we adopt their conclusion that these caspases do indeed help each other downstream of apoptosome formation. In a similar way, our model of the initiator module bears many similarities to the work of Chen et al. and Cui et al. (12,13), and we refer to those articles for more details. Our model also inherits many ideas about time lags and commitment from the work of Albeck et al. (7,19), but we place more emphasis than they do on positive feedback and bistability in the initiator module and the executioner module. We accept their point that programmed cell death is a transient process that need not have (and, indeed, cannot have) a stable steady state of high executioner-caspase activity. Nonetheless, we agree completely with authors of earlier modeling studies that the apoptotic control system must have a stable "OFF" state (the living state) and a distinct threshold stress level for initiating the cell death program. Like the group in Nanjing, China (12,13), we associate the threshold with bistability in the initiator module. We also propose that bistability in the executioner module supports the cell's commitment to apoptosis once caspase 3 is activated. Because our model has bistability in two different stages of the process, neither one of the bistable modules is necessary for a well-orchestrated apoptotic response. But, if both positive feedback loops are compromised, then the cells will no longer be able to make a clear life or death decision, as observed in cells in which both BCL2 and XIAP are disrupted (7).

One of the most remarkable discoveries from recent observations of programmed cell death in single cells is the great

cell-to-cell variability in the latency period between the initial stress signal and the abrupt onset of MOMP (19). Our model attributes this extreme variability to the phenomenon of "critical slowing down" close to a saddle-node bifurcation in the initiator module. The model predicts that, if the positive feedback between BH3 and BAXm is missing (e.g., in a double knock-out of BIM and BID), the activation of BAX is no longer governed by a saddle-node bifurcation (Fig. 9 *A*) and the latency period from cell to cell should now be less variable.

In the initiator module, we propose that BAX activation corresponds to an irreversible transition between stable steady states of low and high BAX activity. This transition serves as a clear signal for downstream events, in particular, the transition of the outer mitochondrial membrane from an impermeable to a highly permeable state (MOMP). Bistability of the BH3-BAX initiator module can be tested by the following experiments.

It may be hard to control a stress signal precisely, but it should be possible to control the level of nondegradable BH3 protein in a cell and thereby to observe bistability in the activation of BAX. In Fig. 9 *A*, we fix total BH3 to different levels and compute the activity of BAX. When $[BH3]_T$ is just above 40, BAX shows bistable activation. To carry out the experiments in vivo, BAX protein could be monitored by a green fluorescent protein tag: inactive BAX molecules are dispersed in the cytoplasm, but active BAX molecules should translocate to the mitochondrial membrane. BH3 proteins could then be injected to activate BAX, and BH3 antibodies could be introduced subsequently to bring the BH3 level down. To prevent cell destruction by active executioner caspases, the experiments should be carried out in cells unable to activate executioner caspases, like cells deficient for both SMAC and CytoC or cells with all caspases inhibited.

A protocol for the experiment in this case could be as follows. Starting from a low BH3 level (Fig. 9 *A*, position *a*), injection of a sufficiently large amount of BH3 will bring the BH3 level to, say, position c, and therefore activate BAX. Later, the right amount of BH3 antibody can be used to bring the BH3 level down to position b. If our picture holds, BAX should stay on the upper branch of the diagram in Fig. 9 *A* and remain activated.

This experiment should be repeated using a slightly different protocol: before injecting BH3 into the cell, it should be preincubated with BH3 antibody. After injecting the mixture into the cell, the BH3 level will go from position a to position b in Fig. 9 *A*, and BAX protein should stay on the lower branch and remain inactive. From these two experiments, one can conclude that, for the BH3 level

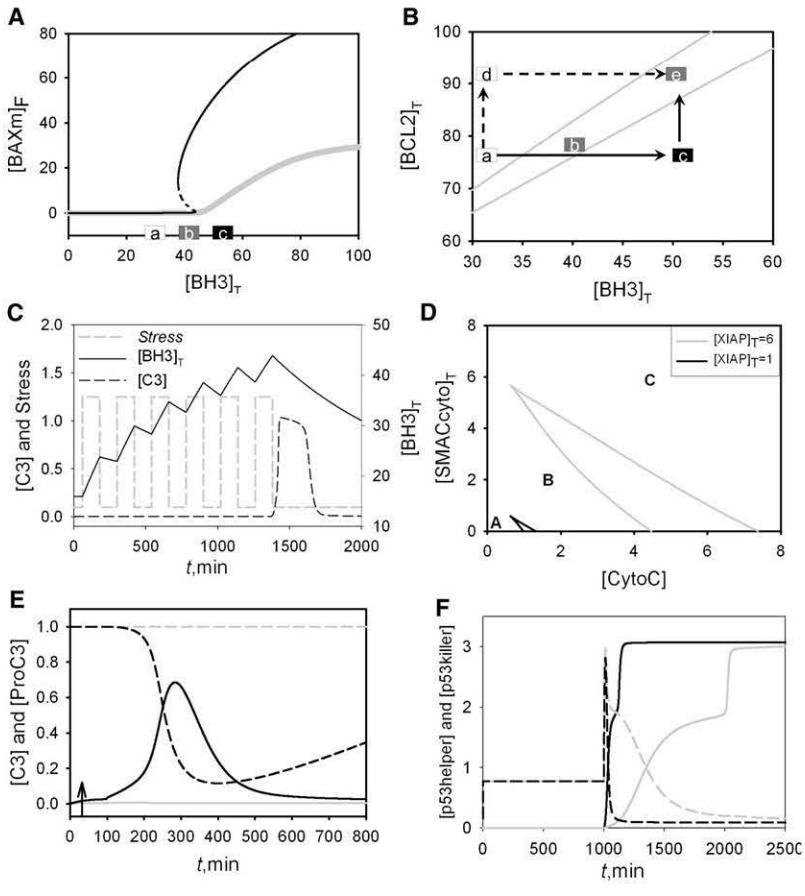

FIGURE 9 Calculations in support of experimental tests of the model. (*A*) One-parameter bifurcation diagram for the initiator module, corresponding to wild-type cells (*black line*) and double-knock-out (*bid* Δ *bim* Δ) mutant (gray line, $k_{f2} = 0$). Solid and dashed lines correspond to stable and unstable steady states, respectively. Note that bistability is lost in the double-knock-out mutant. Points a–c indicate the values of $[BH3]_T$ for the proposed experimental test. Black, white, and gray rectangles indicate active, inactive, and bistable BAXm, respectively. See text for more details. (*B*) Two-parameter bifurcation diagram. *Gray solid lines*, saddle-node bifurcation points; *black solid* and *black dashed lines*, two proposed ways to elevate protein levels. See text for more details. (*C*) Simulated time courses of caspase 3 activity (*black dashed line*) and the level of total BH3 proteins (*black solid line*). A periodic stress signal (*gray dashed line*) is begun at $t = 60$, with Stress = 1.25 for 120 min and Stress = 0.1 for 120 min. The synthesis and degradation rates of BH3 are decreased by 10-fold, $k_s'_{BH3} = 0.01$, $k_s''_{BH3} = 0.06$ and $k_{dBH3} = 0.001$. (*D*) Two-parameter bifurcation diagrams of the model corresponding to wild-type cells ($[XITP]_T = 6$, *gray*) and XIAP deficient cells ($[XIAP]_T = 1$, *black*). (*E*) Simulated time courses of caspase 3 (*solid lines*) and Procaspase 3 (*dashed lines*) corresponding to wild-type cells ($[XITP]_T = 6$, *gray*) and XIAP deficient cells ($[XIAP]_T = 1$, *black*). The initial concentrations of CytoC and SMAC inside the mitochondria are set at 200. Stress = 0.1 for $0 < t < 30$ and Stress = 1 for $t > 30$. (*F*) Simulated time courses of [p53helper] (*dashed lines*) and [p53killer] (*solid lines*) for wild-type cells (*gray*) and DYRK2 mutant cells (*black*). The DYRK2 mutant (enhanced nuclear uptake) is mimicked by setting k_{in} at 0.0015. DNA damage = 0 for $0 < t < 1000$; DNA damage = 10 for $t > 1000$.

of position b, BAX activation is bistable. We cannot state precisely the amounts of BH3 protein and BH3 antibody needed to move the system between points a, b, and c in Fug. 9 *A*, because the current model predicts bistability only as a qualitative feature of the control system. The model is not yet sufficiently calibrated by quantitative data to judge the precise protein levels that define the region of bistability.

If these experiments successfully locate a region of bistability, the information can be used to guide other experiments aiming to test the location of the bistability region in the two-parameter bifurcation diagram (Fig. 9 *B*)—experiments in which both BH3 and BCL2 proteins are to be injected into cells. Our model predicts that BAX activity depends on the sequence in which BH3 and BCL2 are injected. In particular, BAX gets activated if BH3 proteins are injected before BCL2 proteins, which corresponds to the path a → c → e in Fig. 9 *B*. On the contrary, BAX remains inactive if BCL2 proteins are injected before BH3 proteins, which corresponds to the path a → d → e.

Next we propose a series of experiments in which BH3 proteins are induced by pulsatile signals. Pulses of p53 activation (over a period of 5–7 h) after DNA damage have been observed in various settings (70,71). Nonetheless, we are not aware of any experimental work directly addressing the effects of p53 pulses on BH3 protein level. We suggest here two possibilities. First, each p53 pulse induces production of a certain amount of BH3 protein, which may accumulate enough to trigger programmed cell death. The BH3 level in this way "counts" the number of pulses. Because it is the collective contribution of p53 pulses that triggers programmed cell death, we call this possibility the "pulse cooperation route" to apoptosis. Alternatively, the initial pulses of p53 appear predominantly in a p53 helper form, which is inefficient in inducing BH3, and thus the pulses contribute little to BH3 accumulation. As DYRK2 kinase increases in the nucleus, the later pulses of p53 proteins transform into the killer form, which presumably induces enough BH3 to trigger programmed cell death. We call this possibility the "pulse modification route" to apoptosis.

The two routes are not mutually exclusive. The relative contribution of each route depends on the BH3 turnover rate. If BH3 turns over rapidly, its level decreases quickly between p53 pulses, and it is hard for the system to "count" the pulses. This is the case in the model presented here, which relies on the pulse modification route to apoptosis. On the other hand, if BH3 turns over slowly, the pulse cooperation route will play a more significant role. In Fig. 9 *C*, we decrease the rates of BH3 synthesis and degradation by 10-fold, and, as a result, it takes six pulses of p53 to produce enough BH3 to activate caspase 3. (The stress signal in Fig. 9 *C* promotes BH3 production and thus mimics the putative effect of p53 pulses).

The BH3 turnover rate depends on cellular context. For example, the half-life of BIM varies from 3 h to >8 h, depending on whether or not BIM is phosphorylated (72). We suggest that measurement of BH3 turnover in response to p53 pulses in cells undergoing programmed cell death will help to distinguish between the "pulse cooperation" and "pulse modification" routes to apoptosis.

Third, we attribute cell-death commitment to high caspase 3 activity, sustained by slow degradation of SMAC and CytoC. Hence, in our model, the duration of caspase 3 activity is proportional to the initial level of SMAC within mitochondria (simulations not shown). Experiments show that the initial level of SMAC in cells can be increased with external vectors carrying additional copies of the *SMAC* gene or decreased with siRNA, and caspase 3 activation dynamics can be measured in both cases. For example, Albeck et al. decreased SMAC level with siRNA and observed partial cleavage of caspase3 substrates (7), but the duration of caspase 3 activity remains to be measured in future studies.

Fourth, the model reveals three functional regions of the executioner module (Figs. 5 *B* and 9 *D*). In the absence of stress, cells persist in the living state (Fig. 9 *D*, point A) with low caspase 3 activity but plenty of procaspase 3. When stress is applied, cells enter the apoptosis region (point C) to activate caspase 3. In cells deficient for XIAP, the apoptosis region is expanded (Fig. 9 *D*) and less SMAC and CytoC are needed to induce apoptosis. By reducing mitochondrial levels of SMAC and CytoC with siRNAs, one can limit the stimulus of the executioner module to, say, point B in Fig. 9 *D*. For cells with a normal XIAP level, point B is in the living region, and caspase 3 remains inactive. In cells deficient for XIAP, point B is in the apoptosis region, and caspase 3 is activated. The different caspase 3 dynamics in the two cases are shown in Fig. 9 *E*.

Fifth, in the p53 model, nuclear translocation of DYRK2 serves as a "timer" that controls cell fate. Shortly after DNA damage, DYRK2 is mostly cytoplasmic; p53 accumulates in its helper form and induces cell cycle arrest. If DNA damage is sustained, more and more DYRK2 translocates to the nucleus, where p53 transforms to the killer form and induces apoptosis. DYRK2 localization can be manipulated with nuclear export signals and nuclear localization signals. Favoring nuclear localization will accelerate apoptosis (Fig. 9 *F*), whereas favoring nuclear export will delay apoptosis.

Our model of the intrinsic pathway of programmed cell death is intended as a "plug-and-play" subunit of more complex computational models, yet to be developed, of the signaling network of mammalian cells (3). To show how to use the model in this way, we have plugged it into a simple model of the p53 signal processing unit, which receives input from the DNA-damage surveillance mechanism and relays the signal to the cell-cycle control machinery as well as to the programmed cell-death pathway. In the near future, we and other modeling groups will use mathematical models in this way to build more sophisticated, accurate, and predictive simulators of how mammalian cells respond to myriad input signals by appropriate changes in gene expression, movement, cell growth and division, and cell death.

APPENDIX A: EQUATIONS, PARAMETERS AND INITIAL CONDITIONS

Initiator module (four ODEs, 13 parameters, and wiring diagram in Fig. 2 *A*)

$$\frac{d[\mathrm{BAX}]}{dt} = -\left(k_{f1} + k_{f2} \times [\mathrm{BH3}]\right) \times [\mathrm{BAX}] + k_b \times [\mathrm{BAXm}]_\mathrm{F} + k_b \times [\mathrm{BAXm/BCL2}]$$

$$\frac{d[\mathrm{BAXm/BCL2}]}{dt} = k_{\mathrm{asBAXmBCL2}} \times [\mathrm{BAXm}]_\mathrm{F} \times [\mathrm{BCL2}]_\mathrm{F} - k_{\mathrm{dsBAXmBCL2}} \times [\mathrm{BAXm/BCL2}] - k_b \times [\mathrm{BAXm/BCL2}]$$

$$\frac{d[\mathrm{BH3}]_\mathrm{F}}{dt} = k'_{\mathrm{sBH3}} + k''_{\mathrm{sBH3}} \times \mathrm{Stress} - k_{\mathrm{dBH3}} \times [\mathrm{BH3}]_\mathrm{F} - k_{\mathrm{asBH3BCL2}} \times [\mathrm{BH3}]_\mathrm{F} \times [\mathrm{BCL2}]_\mathrm{F} + k_{\mathrm{dsBH3BCL2}} \times [\mathrm{BH3/BCL2}]$$

$$\frac{d[\mathrm{BH3/BCL2}]}{dt} = k_{\mathrm{asBH3BCL2}} \times [\mathrm{BH3}]_\mathrm{F} \times [\mathrm{BCL2}]_\mathrm{F} - k_{\mathrm{dsBH3BCL2}} \times [\mathrm{BH3/BCL2}] - k_{\mathrm{dBH3}} \times [\mathrm{BH3/BCL2}]$$

$$[\mathrm{BAXm}]_\mathrm{F} = [\mathrm{BAX}]_\mathrm{T} - [\mathrm{BAX}] - [\mathrm{BAXm/BCL2}]$$

$$[\mathrm{BCL2}]_\mathrm{F} = [\mathrm{BCL2}]_\mathrm{T} - [\mathrm{BH3/BCL2}] - [\mathrm{BAX_m/BCL2}]$$

$$[\mathrm{BCL2}]_\mathrm{T} = 80, [\mathrm{BAX}]_\mathrm{T} = 100, \mathrm{Stress} = 0.1, k_{f1} = 1,$$

$$k_{f2} = 3, k_b = 2$$

$$k_{\mathrm{asBAXmBCL2}} = 90, k_{\mathrm{dsBAXmBCL2}} = 0.05, k_{\mathrm{asBH3BCL2}} = 10,$$

$$k_{\mathrm{dsBH3BCL2}} = 0.01$$

$$k'_{\mathrm{sBH3}} = 0.1, k''_{\mathrm{sBH3}} = 0.6, k_{\mathrm{dBH3}} = 0.01$$

$$\mathrm{init}\ [\mathrm{BAX}] = 66.6, [\mathrm{BAXm/BCL2}] = 33.4, [\mathrm{BH3}]_\mathrm{F} = 0,$$

$$[\mathrm{BH3/BCL2}] = 16$$

Amplifier module (five ODEs, seven parameters, and wiring diagram in Fig. 2 *B*)

$$\frac{d[\mathrm{CO}]}{dt} = k_{\mathrm{open}} \times [\mathrm{BAXm}]_\mathrm{F}^\mathrm{m} \times \left([\mathrm{C}]_\mathrm{T} - [\mathrm{CO}]\right) - k_{\mathrm{close}} \times [\mathrm{CO}]$$

$$\frac{d[\mathrm{SMAC_{mito}}]}{dt} = -[\mathrm{CO}] \times [\mathrm{SMAC_{mito}}]$$

$$\frac{d[\mathrm{CytoC_{mito}}]}{dt} = -[\mathrm{CO}] \times [\mathrm{CytoC_{mito}}]$$

$$\frac{d[\mathrm{SMAC_{cyto}}]_\mathrm{T}}{dt} = \varepsilon \times [\mathrm{CO}] \times [\mathrm{SMAC_{mito}}] - k_{\mathrm{dSMACcyto}} \times [\mathrm{SMAC}]_\mathrm{F} - k_{\mathrm{dsx}} \times [\mathrm{SMAC/XIAP}]$$

$$\frac{d[\mathrm{CytoC}]}{dt} = \varepsilon \times [\mathrm{CO}] \times [\mathrm{CytoC_{mito}}] - k_{\mathrm{dCYTOC}} \times [\mathrm{CytoC}]$$

$$k_{\mathrm{open}} = 10, m = 4, k_{\mathrm{close}} = 10000, k_{\mathrm{dSMACcyto}} = 0.0001,$$

$$k_{\mathrm{dCYTOC}} = 0.005 \qquad \varepsilon = \frac{V_{\mathrm{mito}}}{V_{\mathrm{cyto}}} = 0.01, [\mathrm{C}]_\mathrm{T} = 1$$

$$\mathrm{init}\ [\mathrm{SMAC_{mito}}] = 1600, [\mathrm{CytoC_{mito}}] = 800,$$

$$[\mathrm{CytoC}] = 0.1, [\mathrm{SMAC_{cyto}}]_\mathrm{T} = 0, [\mathrm{CO}] = 0, \mathrm{where}$$

V represents volume.

Executioner module (eight ODEs, 24 parameters, and wiring diagram in Fig. 2 *C*)

$$d\frac{[\mathrm{ProC9}]}{dt} = k_{\mathrm{sproc9}} - k_{\mathrm{dproc9}} \times [\mathrm{ProC9}] - k_{\mathrm{sc9}} \times [\mathrm{ProC9}] \times [\mathrm{CytoC}]^n$$

$$d\frac{[\mathrm{ProC3}]}{dt} = k_{\mathrm{sproc3}} - k_{\mathrm{dproc3}} \times [\mathrm{ProC3}] - \left(k'_{\mathrm{ac3}} + k''_{\mathrm{ac3}} \times [\mathrm{C9}]^n + k'''_{\mathrm{ac3}} \times [\mathrm{aC9}]^n\right) \times [\mathrm{ProC3}]$$

$$\frac{d[\mathrm{C9}]}{dt} = k_{\mathrm{sC9}} \times [\mathrm{CYTOC}]^n \times [\mathrm{ProC9}] - k_{\mathrm{dc9}} \times [\mathrm{C9}] - \left(k'_{\mathrm{aC9}} + k''_{\mathrm{aC9}} \times [C3]^n\right) \times [\mathrm{C9}] - k_{\mathrm{as9x}} \times [\mathrm{C9}] \times [\mathrm{XIAP}]_\mathrm{F} + k_{\mathrm{ds9x}} \times [\mathrm{XIAP/C9}]$$

$$\frac{d[\mathrm{aC9}]}{dt} = \left(k'_{\mathrm{aC9}} + k''_{\mathrm{aC9}} \times [C3]^n\right) \times [\mathrm{C9}] - k_{\mathrm{dac9}} \times [\mathrm{aC9}]$$

$$\frac{d[C3]}{dt} = \left(k'_{\mathrm{aC3}} + k''_{\mathrm{aC3}} \times [\mathrm{C9}]^n + k'''_{\mathrm{aC3}} \times [\mathrm{aC9}]^n\right) \times ([\mathrm{proC3}]) - k_{\mathrm{dC3}} \times [C3] - k_{\mathrm{as3x}} \times [\mathrm{C3}] \times [\mathrm{XIAP}]_\mathrm{F} + k_{\mathrm{ds3x}} \times [\mathrm{XIAP/C3}]$$

$$\frac{d[\mathrm{XIAP/C9}]}{dt} = k_{\mathrm{as9x}} \times [\mathrm{C9}] \times [\mathrm{XIAP}]_\mathrm{F} - k_{\mathrm{ds9x}} \times [\mathrm{XIAP/C9}] - k_{\mathrm{d9x}} \times [\mathrm{XIAP/C9}]$$

$$\frac{d[\mathrm{XIAP/C3}]}{dt} = k_{\mathrm{as3x}} \times [\mathrm{C3}] \times [\mathrm{XIAP}]_\mathrm{F} - k_{\mathrm{ds3x}} \times [\mathrm{XIAP/C3}] - k_{\mathrm{d3x}} \times [\mathrm{XIAP/C3}]$$

$$\frac{d[\mathrm{SMAC/XIAP}]}{dt} = k_{\mathrm{assx}} \times [\mathrm{SMAC}]_\mathrm{F} \times [\mathrm{XIAP}]_\mathrm{F} - k_{\mathrm{dssx}} \times [\mathrm{SMAC/XIAP}] - k_{\mathrm{dsx}} \times [\mathrm{SMAC/XIAP}]$$

$$[\mathrm{SMAC}]_\mathrm{F} = [\mathrm{SMAC_{cyto}}]_\mathrm{T} - [\mathrm{SMAC/XIAP}]$$

$$[\mathrm{XIAP}]_\mathrm{F} = [\mathrm{XIAP}]_\mathrm{T} - [\mathrm{SMAC/XIAP}] - [\mathrm{XIAP/C3}] - [\mathrm{XIAP/C9}]$$

$$k_{\mathrm{sproc3}} = 0.002, k_{\mathrm{dproc3}} = 0.001, k_{\mathrm{sproc9}} = 0.001,$$

$$k_{\mathrm{dproc9}} = 0.001, k'_{\mathrm{ac9}} = 0.001, k''_{\mathrm{aC9}} = 0.5$$

$k_{sC9} = 0.001,\ k_{dC9} = 0.002,\ k_{daC9} = 0.003,$

$k'_{aC3} = 0.001,\ k''_{aC3} = 0.02,\ k'''_{aC3} = 0.5, n = 2$

$k_{dc3} = 0.002,\ k_{as9x} = 0.1,\ k_{ds9x} = 0.6,\ k_{d9x} = 0.2,$

$k_{as3x} = 0.2,\ k_{ds3x} = 0.5,\ k_{d3x} = 0.1$

$k_{assx} = 2,\ k_{dssx} = 0.01,\ k_{dsx} = 0.007,\ [XIAP]_T = 6$

init $[ProC3] = 1, [ProC9] = 1$

Other variables start from initial values of 0.

*To compute the bifurcation diagrams; set $[C9]_T = 1$ and $[C3]_T = 1$,

and define $[ProC9] = [C9]_T - [C9] - [aC9] - [XIAP/C9]$

and $[ProC3] = [C3]_T - [C3] - [XIAP/C3]$

p53 module (21 ODEs, 70 parameters, and wiring diagram in Fig. 3)

$$\frac{d[DYRK2]}{dt} = k_{in} \times DNAdamage \times \left([DYRK2]_T - [DYRK2]\right) - k_{out} \times [DYRK2]$$

$$\frac{d[p53helper]}{dt} = k_{sp53} - \left(k'_{dp53} + \frac{[MDM2]}{1 + 0.1 \times DNAdamage}\right) \times [p53helper] - \frac{k_{pp53} \times [DYRK2] \times [p53helper]}{J_{pp53} + [p53helper]} + \frac{k_{dpp53} \times [PP] \times [p53killer]}{J_{dpp53} + [p53killer]}$$

$$\frac{d[p53killer]}{dt} = \frac{k_{pp53} \times [DYRK2] \times [p53helper]}{J_{pp53} + [p53helper]} - \frac{k_{dpp53} \times [PP] \times [p53killer]}{J_{dpp53} + [p53killer]} - \left(k'_{dp53} + \frac{[MDM2]}{1 + 0.1 \times DNAdamage}\right) \times [p53killer]$$

$$\frac{d[ASPP]}{dt} = k'_{sASPP} + k''_{sASPP} \times [E2F1] - k_{dASPP} \times [ASPP]$$

$$\frac{d[MDM2]}{dt} = k'_{sMDM2} + k''_{sMDM2} \times [p53]_T - \left(k'_{dMDM2} + k''_{dMDM2} \times DNAdamage\right) \times [MDM2] - k_{asAM} \times [ARF] \times [MDM2] + \left(k_{dsAM} + k_{dARF}\right) \times [ARF/MDM2]$$

$$\frac{d[ARF]}{dt} = k'_{sARF} + k''_{sARF} \times [E2F1] - k_{dARF} \times [ARF] - k_{asAM} \times [ARF] \times [MDM2] + k_{dsAM}[ARF/MDM2] + \left(k'_{dMDM2} + k''_{dMDM2} \times DNAdamage\right) \times [ARF/MDM2]$$

$$\frac{d[ARF/MDM2]}{dt} = k_{asAM} \times [ARF] \times [MDM2] - k_{dsAM}[ARF/MDM2] - \left(k'_{dMDM2} + k''_{dMDM2} \times DNAdamage\right) \times [ARF/MDM2] - k_{dARF} \times [ARF/MDM2]$$

$$\frac{d[CycE]}{dt} = k'_{sE} + k''_{sE} \times [E2F1] - k_{dE} \times [CycE] - k_{asp21E} \times [p21] \times [CycE] + \left(k_{dsp21E} + k_{dp21}\right) \times [p21/CycE]$$

$$\frac{d[E2F1]}{dt} = -k_{asRE} \times [RB] \times [E2F1] + k_{dsRE} \times [RB/E2F1]$$

$$\frac{d[RB_P]}{dt} = \frac{k_{pRB} \times [CycE] \times [RB]}{J_{pRB} + [RB]} - \frac{k_{dpRB} \times [PP] \times [RB_P]}{J_{dpRB} + [RB_P]}$$

$$\frac{d[p21]}{dt} = k'_{sp21} + k''_{sp21} \times [p53helper] + k'''_{sp21} \times [p53killer] - k_{dp21} \times [p21] - k_{asp21E} \times [p21] \times [CycE] + \left(k_{dsp21E} + k_{dE}\right) \times [p21/CycE]$$

$$\frac{d[p21/CycE]}{dt} = k_{asp21E} \times [p21] \times [CycE] - k_{dsp21E} \times [p21/CycE] - k_{dE} \times [p21/CycE] - k_{dp21} \times [p21/CycE]$$

$$\frac{d[\mathrm{BAX}]}{dt} = k_{\mathrm{sBAX}} - k_{\mathrm{dBAX}} \times [\mathrm{BAX}] - \left(k_{f1} + k_{f2} \times [\mathrm{BH3AC}]\right) \times [\mathrm{BAX}] + k_{b1} \times [\mathrm{BAXm}] + k_{b2} \times [\mathrm{BAXm/BCL2}]$$

$$\frac{d[\mathrm{BAXm}]}{dt} = \left(k_{f1} + k_{f2} \times [\mathrm{BH3AC}]\right) \times [\mathrm{BAX}] - k_{b1} \times [\mathrm{BAXm}] - k_{\mathrm{dBAXm}} \times [\mathrm{BAXm}] - k_{\mathrm{asBAXmBCL}} \times [\mathrm{BAXm}] \times [\mathrm{BCL2}] + k_{\mathrm{dsBAXmBCL}} \times [\mathrm{BAXm/BCL2}]$$

$$\frac{d[\mathrm{BCL2}]}{dt} = k_{\mathrm{sBCL2}} - k_{\mathrm{dBCL2}} \times [\mathrm{BCL2}] - k_{\mathrm{asBAXmBCL}} \times [\mathrm{BAXm}] \times [\mathrm{BCL2}] + k_{\mathrm{dsBAXmBCL}} \times [\mathrm{BAXm/BCL2}] - k_{\mathrm{asBH3ACBCL}} \times [\mathrm{BH3AC}] \times [\mathrm{BCL2}] + k_{\mathrm{dsBH3ACBCL}} \times [\mathrm{BH3AC/BCL2}] - k_{\mathrm{asBH3DRBCL}} \times [\mathrm{BH3DR}] \times [\mathrm{BCL2}] + k_{\mathrm{dsBH3DRBCL}} \times [\mathrm{BH3DR/BCL2}] + k_{b2} \times [\mathrm{BAXm/BCL2}]$$

$$\frac{d[\mathrm{BH3AC}]}{dt} = k_{\mathrm{sBH3AC}} - k_{\mathrm{dBH3AC}} \times [\mathrm{BH3AC}] - k_{\mathrm{asBH3ACBCL}} \times [\mathrm{BH3AC}] \times [\mathrm{BCL2}] + k_{\mathrm{dsBH3ACBCL}} \times [\mathrm{BH3AC/BCL2}]$$

$$\frac{d[\mathrm{BH3DR}]}{dt} = k_{\mathrm{sBH3DR}} - k_{\mathrm{dBH3DR}} \times [\mathrm{BH3DR}] - k_{\mathrm{asBH3DRBCL}} \times [\mathrm{BH3R}] \times [\mathrm{BCL2}] + k_{\mathrm{dsBH3DRBCL}} \times [\mathrm{BH3DR/BCL2}]$$

$$\frac{d[\mathrm{BAXm/BCL2}]}{dt} = k_{\mathrm{asBAXmBCL}} \times [\mathrm{BAXm}] \times [\mathrm{BCL2}] - k_{\mathrm{dsBAXmBCL}} \times [\mathrm{BAXm/BCL2}] - k_{b2} \times [\mathrm{BAXm/BCL2}] - k_{\mathrm{dBAXmBCL}} \times [\mathrm{BAXm/BCL2}]$$

$$\frac{d[\mathrm{BH3AC/BCL2}]}{dt} = k_{\mathrm{asBH3ACBCL}} \times [\mathrm{BH3AC}] \times [\mathrm{BCL2}] - k_{\mathrm{dsBH3ACBCL}} \times [\mathrm{BH3AC/BCL2}] - k_{\mathrm{dBH3ACBCL}} \times [\mathrm{BH3AC/BCL2}]$$

$$\frac{d[\mathrm{BH3DR/BCL2}]}{dt} = k_{\mathrm{asBH3DRBCL}} \times [\mathrm{BH3DR}] \times [\mathrm{BCL2}] - k_{\mathrm{dsBH3DRBCL}} \times [\mathrm{BH3DR/BCL2}] - k_{\mathrm{dBH3DRBCL}} \times [\mathrm{BH3DR/BCL2}]$$

$$\frac{\mathrm{d}[\mathrm{p73}]}{dt} = k'_{\mathrm{sp73}} + k''_{\mathrm{sp73}} \times [\mathrm{E2F1}] - k_{\mathrm{dp73}} \times [\mathrm{p73}]$$

$$[\mathrm{p53}]_{\mathrm{T}} = [\mathrm{p53helper}] + [\mathrm{p53killer}]$$

$$[\mathrm{RB/E2F1}] = [\mathrm{E2F1}]_{\mathrm{T}} - [\mathrm{E2F1}]$$

$$[\mathrm{RB}] = [\mathrm{RB}]_{\mathrm{T}} - [\mathrm{RB_P}] - [\mathrm{RB/E2F1}]$$

$$k_{\mathrm{sBH3AC}} = k'_{\mathrm{sBH3AC}} + k''_{\mathrm{sBH3AC}} \times (1 + [\mathrm{ASPP}]) \times [\mathrm{p53killer}] + k'''_{\mathrm{sBH3AC}} \times [\mathrm{p73}] + k''''_{\mathrm{sBH3AC}} \times (1 + [\mathrm{ASPP}]) \times [\mathrm{p53helper}]$$

$$k_{\mathrm{sBH3DR}} = k'_{\mathrm{sBH3DR}} + k''_{\mathrm{sBH3DR}} \times (1 + [\mathrm{ASPP}]) \times [\mathrm{p53killer}] + k'''_{\mathrm{sBH3DR}} \times [\mathrm{p73}] + k''''_{\mathrm{sBH3DR}} \times (1 + [\mathrm{ASPP}]) \times [\mathrm{p53helper}]$$

$k_{\mathrm{in}} = 0.00015$, $k_{\mathrm{out}} = 0.0003$, $[\mathrm{DYRK2}]_{\mathrm{T}} = 2$, $k_{\mathrm{sp53}} = 0.5$, $k'_{\mathrm{dp53}} = 0.1$, $k_{\mathrm{pp53}} = 1$

$J_{\mathrm{pp53}} = 0.1$, $k_{\mathrm{dpp53}} = 0.5$, $J_{\mathrm{dpp53}} = 0.1$, $[\mathrm{PP}] = 1$, $k'_{\mathrm{sASPP}} = 0.01$, $k''_{\mathrm{sASPP}} = 0.05$, $k_{\mathrm{dASPP}} = 0.1$

$k'_{\mathrm{sMDM2}} = 0.02$, $k''_{\mathrm{sMDM2}} = 0.3$, $k'_{\mathrm{dMDM2}} = 0.1$, $k''_{\mathrm{dMDM2}} = 0.1$, $k'_{\mathrm{sARF}} = 0.01$, $k''_{\mathrm{sARF}} = 0.3$, $k_{\mathrm{dARF}} = 0.1$

$k_{\mathrm{asAM}} = 10$, $k_{\mathrm{dsAM}} = 2$, $k'_{\mathrm{sE}} = 0.01$, $k''_{\mathrm{sE}} = 0.5$, $k_{\mathrm{dE}} = 0.12$, $k_{\mathrm{asRE}} = 5$, $k_{\mathrm{dsRE}} = 1$, $k_{\mathrm{pRB}} = 1$

$J_{\mathrm{pRB}} = 0.1$, $k_{\mathrm{dpRB}} = 0.5$, $J_{\mathrm{dpRB}} = 0.1$, $[\mathrm{RB}]_{\mathrm{T}} = 2$, $[\mathrm{E2F1}]_{\mathrm{T}} = 1$, $k'_{\mathrm{sp21}} = 0.03$, $k''_{\mathrm{sp21}} = 0.3$

$k'''_{\mathrm{sp21}} = 0.01$, $k_{\mathrm{dp21}} = 0.2$, $k_{\mathrm{asp21E}} = 10$, $k_{\mathrm{dsp21E}} = 1$, $k_{\mathrm{sBAX}} = 0.97$, $k_{\mathrm{dBAX}} = 0.01$, $k_{f1} = 0.1$

$k_{f2} = 3.4$, $k_{b1} = 4.2$, $k_{b2} = 4.2$, $k_{\mathrm{dBAXm}} = 0.01$, $k_{\mathrm{asBAXmBCL}} = 87$, $k_{\mathrm{dsBAXmBCL}} = 0.05$

$k_{sBCL2} = 0.57$, $k_{dBCL2} = 0.01$, $k_{asBH3ACBCL} = 11.14$, $k_{dsBH3ACBCL} = 0.01$, $k_{asBH3DRBCL} = 11.14$

$k_{dsBH3DRBCL} = 0.01$, $k_{dBH3AC} = 0.01$, $k_{dBH3DR} = 0.01$, $k_{dBAXmBCL} = 0.01$, $k_{dBH3ACBCL} = 0.01$

$k_{dBH3DRBCL} = 0.01$, $k'_{sp73} = 0.01$, $k''_{sp73} = 0.01$, $k_{dp73} = 0.5$, $k'_{sBH3AC} = 0.01$, $k''_{sBH3AC} = 0.05$

$k'''_{sBH3AC} = 0.1$, $k''''_{sBH3AC} = 0.02$, $k'_{sBH3DR} = 0.01$, $k''_{sBH3DR} = 0.1$, $k'''_{sBH3DR} = 0.1$, $k''''_{sBH3DR} = 0.02$

init $[BAX] = 95$, $[p53]_T = 0.78$, $[ASPP] = 0.55$, $[MDM2]_T = 2.53$

init $[ARF]_T = 2.79$, $[ARF/MDM2] = 1.99$, $[CycE]_T = 3.83$, $[E2F1] = 0.9$

init $[RB_P] = 1.88$, $[p21]_T = 1.32$, $[p21/CycE] = 1.25$, $[BCL2] = 47.49$

init $[BAXm/BCL2] = 2.26$, $[BH3AC/BCL2] = 3.78$, $[BH3DR/BCL2] = 3.78$, $[p73] = 0.04$

APPENDIX B: IT IS INVALID TO ASSUME BAXM IS INACTIVATED ONLY FROM THE MONOMER FORM

If we assume that BAXm gets inactivated only from the monomer form, then in resting cells (with [BH3] ≈ 0), the concentration of BAXm will be controlled by the rate equations

$$\frac{d[\mathrm{BAXm}]_F}{dt} = k_{f1} \times [\mathrm{BAX}] - k_b \times [\mathrm{BAXm}]_F - k_{asBAXmBCL2} \times [\mathrm{BAXm}]_F \times [\mathrm{BCL2}]_F + k_{dsBAXmBCL2} \times [\mathrm{BAXm/BCL2}]$$

$$\frac{d[\mathrm{BAXm/BCL2}]}{dt} = k_{asBAXmBCL2} \times [\mathrm{BAXm}]_F \times [\mathrm{BCL2}]_F - k_{dsBAXmBCL2} \times [\mathrm{BAXm/BCL2}],$$

where [BAX] = [BAX]T − [BAXm]F − [BAXm/BCL2] and [BCL2]F = [BCL2]T − [BAXm/BCL2]. At steady state, the concentrations of BAXm monomer and BAXm/BCL2 dimer are

$$[\mathrm{BAXm}]_F = \frac{2K_d[\mathrm{BAX}]_T}{\sqrt{B^2 + 4AK_d} + B}, \quad [\mathrm{BAXm/BCL2}] = [\mathrm{BAX}]_T - \left(1 + \frac{k_b}{k_{f1}}\right)[\mathrm{BAXm}]_F$$

where $A = \left(1 + \frac{k_b}{k_{f1}}\right)[\mathrm{BAX}]_T$, $B = [\mathrm{BCL2}]_T - [\mathrm{BAX}]_T + K_d\left(1 + \frac{k_b}{k_{f1}}\right)$, and $K_d = \frac{k_{dsBAXmBCL2}}{k_{asBAXmBCL2}}$. It is reasonable to assume that BCL2 binds tightly to BAXm, i.e., $K_d \ll [\mathrm{BAX}]_T$, in which case, $\sqrt{B^2 + 4AK_d} \approx |B| + \frac{2AK_d}{|B|}$. If $[\mathrm{BAX}]_T < [\mathrm{BCL2}]_T$, i.e., $B > 0$, then $[\mathrm{BAXm}]_F \approx 0$ and $[\mathrm{BAXm/BCL2}] \approx [\mathrm{BAX}]_T$. In this case, in a resting cell, all BAX molecules pile up in the mitochondrial membrane in combination with BCL2, in contradiction to the fact that most BAX stays in the cytoplasm of resting cells (73,74).

To keep most BAX in the cytoplasm, we would have to assume that $[\mathrm{BAX}]_T > [\mathrm{BCL2}]_T$, i.e., $B < 0$, in which case $[\mathrm{BAXm}]_F \cong \frac{[\mathrm{BAX}]_T - [\mathrm{BCL2}]_T}{1 + k_b/k_{f1}}$. To keep $[\mathrm{BAXm}]_F$ low in a resting cell (to avoid accidental apoptosis), k_b must be much larger than k_{f1}. In this case, it is very difficult for BH3 proteins to activate BAX, because the rate of spontaneous inactivation is very large. In our opinion, this is an unlikely scenario for control of apoptosis.

Based on these considerations, we assume that BAXm can be inactivated equally well as monomers and as dimers in combination with BCL2.

SUPPORTING MATERIAL

ode files are available at http://www.biophysj.org/biophysj/supplemental/S0006-3495(09)00970-9.

Tongli Zhang thanks John Albeck, John Burke, and Peter Sorger for sharing their unpublished ideas and data, and Kathy Chen, Stefan Legewie, and Zerrin Bagci for stimulating discussions.

This research was supported by grants from the United States National Science Foundation to P.B. (DMS-0342283) and to K.I.T.P. (PHY05-51164) and from Virginia Polytechnic Institute's Institute for Critical Technologies and Applied Science to J.J.T.

REFERENCES

1. Johnstone, R. W., A. A. Ruefli, and S. W. Lowe. 2002. Apoptosis: a link between cancer genetics and chemotherapy. *Cell.* 108:153–164.
2. Fulda, S., and K. M. Debatin. 2006. Extrinsic versus intrinsic apoptosis pathways in anticancer chemotherapy. *Oncogene.* 25:4798–4811.
3. Hanahan, D., and R. A. Weinberg. 2000. The hallmarks of cancer. *Cell.* 100:57–70.
4. Weinberg, R. A. 2007. The Biology of Cancer. Garland Science, New York.
5. Green, D. R. 2000. Apoptotic pathways: paper wraps stone blunts scissors. *Cell.* 102:1–4.
6. Meng, X. W., S. H. Lee, and S. H. Kaufmann. 2006. Apoptosis in the treatment of cancer: a promise kept? *Curr. Opin. Cell Biol.* 18:668–676.
7. Albeck, J. G., J. M. Burke, B. B. Aldridge, M. Zhang, D. A. Lauffenburger, et al. 2008. Quantitative analysis of pathways controlling extrinsic apoptosis in single cells. *Mol. Cell.* 30:11–25.
8. Rehm, M., H. Dussmann, R. U. Janicke, J. M. Tavare, D. Kogel, et al. 2002. Single-cell fluorescence resonance energy transfer analysis

demonstrates that caspase activation during apoptosis is a rapid process. Role of caspase-3. *J. Biol. Chem.* 277:24506–24514.

9. Aldridge, B. B., G. Haller, P. K. Sorger, and D. A. Lauffenburger. 2006. Direct Lyapunov exponent analysis enables parametric study of transient signalling governing cell behaviour. *IEE Syst. Biol.* 153:425–432.
10. Bagci, E. Z., Y. Vodovotz, T. R. Billiar, G. B. Ermentrout, and I. Bahar. 2006. Bistability in apoptosis: roles of bax, bcl-2, and mitochondrial permeability transition pores. *Biophys. J.* 90:1546–1559.
11. Bentele, M., I. Lavrik, M. Ulrich, S. Stosser, D. W. Heermann, et al. 2004. Mathematical modeling reveals threshold mechanism in CD95-induced apoptosis. *J. Cell Biol.* 166:839–851.
12. Chen, C., J. Cui, H. Lu, R. Wang, S. Zhang, et al. 2007. Modeling of the role of a Bax-activation switch in the mitochondrial apoptosis decision. *Biophys. J.* 92:4304–4315.
13. Cui, J., C. Chen, H. Lu, T. Sun, and P. Shen. 2008. Two independent positive feedbacks and bistability in the bcl-2 apoptotic switch. *PLoS ONE.* 3:e1469.
14. Eissing, T., H. Conzelmann, E. D. Gilles, F. Allgower, E. Bullinger, et al. 2004. Bistability analyses of a caspase activation model for receptor-induced apoptosis. *J. Biol. Chem.* 279:36892–36897.
15. Fussenegger, M., J. E. Bailey, and J. Varner. 2000. A mathematical model of caspase function in apoptosis. *Nat. Biotechnol.* 18:768–774.
16. Hua, F., M. G. Cornejo, M. H. Cardone, C. L. Stokes, and D. A. Lauffenburger. 2005. Effects of Bcl-2 levels on Fas signaling-induced caspase-3 activation: molecular genetic tests of computational model predictions. *J. Immunol.* 175:985–995.
17. Legewie, S., N. Bluthgen, and H. Herzel. 2006. Mathematical modeling identifies inhibitors of apoptosis as mediators of positive feedback and bistability. *PLoS Comput. Biol.* 2:e120.
18. Rehm, M., H. J. Huber, H. Dussmann, and J. H. Prehn. 2006. Systems analysis of effector caspase activation and its control by X-linked inhibitor of apoptosis protein. *EMBO J.* 25:4338–4349.
19. Albeck, J. G., J. M. Burke, S. L. Spencer, D. A. Lauffenburger, and P. K. Sorger. 2008. Modeling a snap-action, variable-delay switch controlling extrinsic cell death. *PLoS Biol.* 6:2831–2852.
20. Elledge, R. M., and W. H. Lee. 1995. Life and death by p53. *Bioessays.* 17:923–930.
21. Lu, X. 2005. p53: a heavily dictated dictator of life and death. *Curr. Opin. Genet. Dev.* 15:27–33.
22. Michalak, E., A. Villunger, M. Erlacher, and A. Strasser. 2005. Death squads enlisted by the tumour suppressor p53. *Biochem. Biophys. Res. Commun.* 331:786–798.
23. Chipuk, J. E., and D. R. Green. 2006. Dissecting p53-dependent apoptosis. *Cell Death Differ.* 13:994–1002.
24. Desagher, S., A. Osen-Sand, A. Nichols, R. Eskes, S. Montessuit, et al. 1999. Bid-induced conformational change of Bax is responsible for mitochondrial cytochrome *c* release during apoptosis. *J. Cell Biol.* 144:891–901.
25. Eskes, R., S. Desagher, B. Antonsson, and J. C. Martinou. 2000. Bid induces the oligomerization and insertion of Bax into the outer mitochondrial membrane. *Mol. Cell. Biol.* 20:929–935.
26. Marani, M., T. Tenev, D. Hancock, J. Downward, and N. R. Lemoine. 2002. Identification of novel isoforms of the BH3 domain protein Bim which directly activate Bax to trigger apoptosis. *Mol. Cell. Biol.* 22:3577–3589.
27. Chipuk, J. E., L. Bouchier-Hayes, and D. R. Green. 2006. Mitochondrial outer membrane permeabilization during apoptosis: the innocent bystander scenario. *Cell Death Differ.* 13:1396–1402.
28. Green, D. R. 2005. Apoptotic pathways: ten minutes to dead. *Cell.* 121:671–674.
29. Riedl, S. J., and Y. Shi. 2004. Molecular mechanisms of caspase regulation during apoptosis. *Nat. Rev. Mol. Cell Biol.* 5:897–907.
30. Holcik, M., and R. G. Korneluk. 2001. XIAP, the guardian angel. *Nat. Rev. Mol. Cell Biol.* 2:550–556.
31. Cummins, J. M., M. Kohli, C. Rago, K. W. Kinzler, B. Vogelstein, et al. 2004. X-linked inhibitor of apoptosis protein (XIAP) is a nonredundant modulator of tumor necrosis factor-related apoptosis-inducing ligand (TRAIL)-mediated apoptosis in human cancer cells. *Cancer Res.* 64:3006–3008.
32. Lakhani, S. A., A. Masud, K. Kuida, G. A. Porter, Jr., C. J. Booth, et al. 2006. Caspases 3 and 7: key mediators of mitochondrial events of apoptosis. *Science.* 311:847–851.
33. Finucane, D. M., E. Bossy-Wetzel, N. J. Waterhouse, T. G. Cotter, and D. R. Green. 1999. Bax-induced caspase activation and apoptosis via cytochrome *c* release from mitochondria is inhibitable by Bcl-xL. *J. Biol. Chem.* 274:2225–2233.
34. Murphy, K. M., V. Ranganathan, M. L. Farnsworth, M. Kavallaris, and R. B. Lock. 2000. Bcl-2 inhibits Bax translocation from cytosol to mitochondria during drug-induced apoptosis of human tumor cells. *Cell Death Differ.* 7:102–111.
35. Shiozaki, E. N., J. Chai, and Y. Shi. 2002. Oligomerization and activation of caspase-9, induced by Apaf-1 CARD. *Proc. Natl. Acad. Sci. USA.* 99:4197–4202.
36. Srinivasula, S. M., M. Ahmad, T. Fernandes-Alnemri, and E. S. Alnemri. 1998. Autoactivation of procaspase-9 by Apaf-1-mediated oligomerization. *Mol. Cell.* 1:949–957.
37. Zou, H., R. Yang, J. Hao, J. Wang, C. Sun, et al. 2003. Regulation of the Apaf-1/caspase-9 apoptosome by caspase-3 and XIAP. *J. Biol. Chem.* 278:8091–8098.
38. Suzuki, Y., Y. Nakabayashi, and R. Takahashi. 2001. Ubiquitin-protein ligase activity of X-linked inhibitor of apoptosis protein promotes proteasomal degradation of caspase-3 and enhances its anti-apoptotic effect in Fas-induced cell death. *Proc. Natl. Acad. Sci. USA.* 98:8662–8667.
39. MacFarlane, M., W. Merrison, S. B. Bratton, and G. M. Cohen. 2002. Proteasome-mediated degradation of Smac during apoptosis: XIAP promotes Smac ubiquitination in vitro. *J. Biol. Chem.* 277:36611–36616.
40. Shiozaki, E. N., J. Chai, D. J. Rigotti, S. J. Riedl, P. Li, et al. 2003. Mechanism of XIAP-mediated inhibition of caspase-9. *Mol. Cell.* 11:519–527.
41. Sharpless, N. E., and R. A. DePinho. 2007. Cancer biology: gone but not forgotten. *Nature.* 445:606–607.
42. Harris, S. L., and A. J. Levine. 2005. The p53 pathway: positive and negative feedback loops. *Oncogene.* 24:2899–2908.
43. Mowat, M. R. 1998. p53 in tumor progression: life, death, and everything. *Adv. Cancer Res.* 74:25–48.
44. Oren, M. 2003. Decision making by p53: life, death and cancer. *Cell Death Differ.* 10:431–442.
45. Sherr, C. J. 1998. Tumor surveillance via the ARF-p53 pathway. *Genes Dev.* 12:2984–2991.
46. Olsson, A., C. Manzl, A. Strasser, and A. Villunger. 2007. How important are post-translational modifications in p53 for selectivity in target-gene transcription and tumour suppression? *Cell Death Differ.* 14:1561–1575.
47. Csikasz-Nagy, A., D. Battogtokh, K. C. Chen, B. Novak, and J. J. Tyson. 2006. Analysis of a generic model of eukaryotic cell-cycle regulation. *Biophys. J.* 90:4361–4379.
48. Zhang, T., P. Brazhnik, and J. J. Tyson. 2007. Exploring mechanisms of the DNA-damage response: p53 pulses and their possible relevance to apoptosis. *Cell Cycle.* 6:85–94.
49. Yu, J., and L. Zhang. 2003. No PUMA, no death: implications for p53-dependent apoptosis. *Cancer Cell.* 4:248–249.
50. Dynlacht, B. D. 2005. E2F and p53 make a nice couple: converging pathways in apoptosis. *Cell Death Differ.* 12:313–314.
51. Ginsberg, D. 2007. EGFR signaling inhibits E2F1-induced apoptosis in vivo: implications for cancer therapy. *Sci. STKE.* 2007:pe4.
52. Irwin, M., M. C. Marin, A. C. Phillips, R. S. Seelan, D. I. Smith, et al. 2000. Role for the p53 homologue p73 in E2F–1-induced apoptosis. *Nature.* 407:645–648.

53. Braithwaite, A. W., G. Del Sal, and X. Lu. 2006. Some p53-binding proteins that can function as arbiters of life and death. *Cell Death Differ.* 13:984–993.

54. Furukawa, Y., N. Nishimura, Y. Furukawa, M. Satoh, H. Endo, et al. 2002. Apaf-1 is a mediator of E2F-1-induced apoptosis. *J. Biol. Chem.* 277:39760–39768.

55. Nahle, Z., J. Polakoff, R. V. Davuluri, M. E. McCurrach, M. D. Jacobson, et al. 2002. Direct coupling of the cell cycle and cell death machinery by E2F. *Nat. Cell Biol.* 4:859–864.

56. Bode, A. M., and Z. Dong. 2004. Post-translational modification of p53 in tumorigenesis. *Nat. Rev. Cancer.* 4:793–805.

57. Toledo, F., and G. M. Wahl. 2006. Regulating the p53 pathway: in vitro hypotheses, in vivo veritas. *Nat. Rev. Cancer.* 6:909–923.

58. Aylon, Y., and M. Oren. 2007. Living with p53, dying of p53. *Cell.* 130:597–600.

59. Taira, N., K. Nihira, T. Yamaguchi, Y. Miki, and K. Yoshida. 2007. DYRK2 is targeted to the nucleus and controls p53 via Ser46 phosphorylation in the apoptotic response to DNA damage. *Mol. Cell.* 25:725–738.

60. Brazhnik, P., and J. J. Tyson. 2006. Cell cycle control in bacteria and yeast: a case of convergent evolution? *Cell Cycle.* 5:522–529.

61. Chen, K. C., L. Calzone, A. Csikasz-Nagy, F. R. Cross, B. Novak, et al. 2004. Integrative analysis of cell cycle control in budding yeast. *Mol. Biol. Cell.* 15:3841–3862.

62. Eissing, T., F. Allgower, and E. Bullinger. 2005. Robustness properties of apoptosis models with respect to parameter variations and intrinsic noise. *Syst. Biol.* (Stevenage). 152:221–228.

63. Goldstein, J. C., N. J. Waterhouse, P. Juin, G. I. Evan, and D. R. Green. 2000. The coordinate release of cytochrome *c* during apoptosis is rapid, complete and kinetically invariant. *Nat. Cell Biol.* 2:156–162.

64. Chandra, D., J. W. Liu, and D. G. Tang. 2002. Early mitochondrial activation and cytochrome *c* up-regulation during apoptosis. *J. Biol. Chem.* 277:50842–50854.

65. Green, D. R., and J. C. Reed. 1998. Mitochondria and apoptosis. *Science.* 281:1309–1312.

66. Martin, A. G., and H. O. Fearnhead. 2002. Apocytochrome *c* blocks caspase-9 activation and Bax-induced apoptosis. *J. Biol. Chem.* 277:50834–50841.

67. Willis, S. N., J. I. Fletcher, T. Kaufmann, M. F. van Delft, L. Chen, et al. 2007. Apoptosis initiated when BH3 ligands engage multiple Bcl-2 homologs, not Bax or Bak. *Science.* 315:856–859.

68. Harlin, H., S. B. Reffey, C. S. Duckett, T. Lindsten, and C. B. Thompson. 2001. Characterization of XIAP-deficient mice. *Mol. Cell. Biol.* 21:3604–3608.

69. Seoane, J., H. V. Le, and J. Massague. 2002. Myc suppression of the p21(Cip1) Cdk inhibitor influences the outcome of the p53 response to DNA damage. *Nature.* 419:729–734.

70. Geva-Zatorsky, N., N. Rosenfeld, S. Itzkovitz, R. Milo, A. Sigal, E. Dekel, T. Yarnitzky, Y. Liron, P. Polak, G. Lahav, and U. Alon. 2006. Oscillations and variability in the p53 system. *Mol. Syst. Biol.* 2:2006.0033.

71. Hamstra, D. A., M. S. Bhojani, L. B. Griffin, B. Laxman, B. D. Ross, et al. 2006. Real-time evaluation of p53 oscillatory behavior in vivo using bioluminescent imaging. *Cancer Res.* 66:7482–7489.

72. Ley, R., K. Balmanno, K. Hadfield, C. Weston, and S. J. Cook. 2003. Activation of the ERK1/2 signaling pathway promotes phosphorylation and proteasome-dependent degradation of the BH3-only protein, Bim. *J. Biol. Chem.* 278:18811–18816.

73. Schuler, M., U. Maurer, J. C. Goldstein, F. Breitenbucher, S. Hoffarth, et al. 2003. p53 triggers apoptosis in oncogene-expressing fibroblasts by the induction of Noxa and mitochondrial Bax translocation. *Cell Death Differ.* 10:451–460.

74. Smaili, S. S., Y. T. Hsu, K. M. Sanders, J. T. Russell, and R. J. Youle. 2001. Bax translocation to mitochondria subsequent to a rapid loss of mitochondrial membrane potential. *Cell Death Differ.* 8:909–920.